JAMES | Journal of Advances in Modeling Earth Systems

RESEARCH ARTICLE
10.1029/2023MS003976

Investigating Mountain Watershed Headwater-To-Groundwater Connections, Water Sources, and Storage Selection Behavior With Dynamic-Flux Particle Tracking

P. James Dennedy-Frank[1,2], **Ate Visser**[3], **Fadji Z. Maina**[1,4], **and Erica R. Siirila-Woodburn**[1]

[1]Lawrence Berkeley National Laboratory, Earth and Environmental Sciences Area, Oakland, CA, USA, [2]Now at Department of Marine & Environmental Science, Northeastern University, Boston, MA, USA, [3]Lawrence Livermore National Laboratory, Livermore, CA, USA, [4]Now at NASA Goddard Spaceflight Center, Greenbelt, MD, USA

Key Points:

- Dynamic-flux particle tracking (DFPT) is a novel technique to investigate watershed function and connection
- Water source wedge plots illustrate connectivity between source water elevation, precipitation phase, and water exit pathways and location
- DFPT shows how source phase and watershed conditions influence age-ranked storage selection behavior

Supporting Information:

Supporting Information may be found in the online version of this article.

Correspondence to:

P. J. Dennedy-Frank,
pjdf@northeastern.edu

Citation:

Dennedy-Frank, P. J., Visser, A., Maina, F. Z., & Siirila-Woodburn, E. R. (2024). Investigating mountain watershed headwater-to-groundwater connections, water sources, and storage selection behavior with dynamic-flux particle tracking. *Journal of Advances in Modeling Earth Systems*, *16*, e2023MS003976. https://doi.org/10.1029/2023MS003976

Received 21 AUG 2023
Accepted 26 JUN 2024

Author Contributions:

Conceptualization: P. James Dennedy-Frank, Ate Visser, Erica R. Siirila-Woodburn
Data curation: P. James Dennedy-Frank
Formal analysis: P. James Dennedy-Frank, Ate Visser, Erica R. Siirila-Woodburn
Funding acquisition: Ate Visser, Erica R. Siirila-Woodburn
Investigation: P. James Dennedy-Frank, Ate Visser, Fadji Z. Maina, Erica R. Siirila-Woodburn
Methodology: P. James Dennedy-Frank, Ate Visser, Erica R. Siirila-Woodburn

Abstract Climate change will impact mountain watershed streamflow both directly—with changing precipitation amounts and variability—and indirectly—through temperature shifts altering snowpack, melt, and evapotranspiration. To understand how these complex processes will affect ecosystem functioning and water resources, we need tools to distinguish connections between water sources (rain/snowmelt), groundwater storage, and exit fluxes (streamflow/evapotranspiration), and to determine how these connections change seasonally and as climate shifts. Here, we develop novel watershed-scale approaches to understand water source, storage, and exit flux connections using a dynamic-flux particle tracking model (EcoSLIM) applied in California's Cosumnes Watershed, which connects the Sierra Nevada and Central Valley. This work develops new visualizations and applications to provide mechanistic understanding that underpins the interpretation of isotopic field data at watershed scales to distinguish sources, flow paths, residence times, and storage selection. In our simulations, streamflow comes primarily from snow-derived water while evapotranspiration generally comes from rain. Most streamflow starts above 1,000 m while evapotranspiration is sourced relatively evenly across the watershed and is generally younger than streamflow. Modeled streamflow consists primarily of water sourced from precipitation in the previous 5 years but before the current water year, while ET consists primarily of water from precipitation in the current water year. ET, and to a lesser extent streamflow, are both younger than water in groundwater storage. However, snowmelt-derived streamflow preferentially discharges older water from snow-derived storage. Dynamic-flux particle tracking and new approaches presented here enable novel model-tracer comparisons in large-scale watersheds to better understand watershed behavior in a changing climate.

Plain Language Summary Climate change will alter the hydrologic cycle: storms will be more intense and higher temperatures will result in less snow, earlier melt, and more early-season water use by plants. To understand the combined effect of these changes, we need models to simulate water flows and precisely study the effects of rain, snowmelt, subsurface storage, streamflow, and plant water uptake. These models can show us how water flows between different components of the landscape, and how this flow changes seasonally and in response to climate change. This study develops new modeling tools that simulate the Cosumnes River in the Sierra Nevada (California, USA) and will help interpret field data at watershed scales. The majority of simulated streamflow originates from snow while plants rely on rainfall for evapotranspiration (ET). Most streamflow starts as precipitation above 1,000 m while ET comes from water that falls evenly across the watershed. Water used for ET is generally younger than streamflow: most streamflow is 1–5 years old, while most ET is less than 1 year old. Both ET and streamflow are younger than water stored in the subsurface. These new modeling tools, called dynamic-flux particle tracking, will help us predict how watersheds will behave as climate changes.

1. Introduction

Water resource systems are experiencing changes in climate and associated shifts in vegetation and human water use; to develop resilient systems in a continuously changing world, we need to understand how water flows through watersheds over space and time (Barnett et al., 2005; Milly & Dunne, 2020; Siirila-Woodburn et al., 2021). Changes in precipitation amounts and variability, as well as temperature averages, extremes, and timing, will directly alter water fluxes and indirectly change ecosystems and human water management and thus

Project administration: Erica R. Siirila-Woodburn
Resources: Ate Visser, Erica R. Siirila-Woodburn
Software: P. James Dennedy-Frank, Fadji Z. Maina
Supervision: Erica R. Siirila-Woodburn
Validation: P. James Dennedy-Frank, Erica R. Siirila-Woodburn
Visualization: P. James Dennedy-Frank, Ate Visser, Erica R. Siirila-Woodburn
Writing – original draft: P. James Dennedy-Frank, Ate Visser, Erica R. Siirila-Woodburn
Writing – review & editing: P. James Dennedy-Frank, Ate Visser, Erica R. Siirila-Woodburn

water fluxes. Traditional empirical relationships for predicting watershed response may not hold (Milly et al., 2008). We need to better understand the physical links between water sources (rain/snowmelt), fluxes and exit pathways (streamflow/evapotranspiration), and groundwater storage to determine how they will shift with the climate. Approaches that characterize these links will build understanding of fundamental watershed function and help us better manage water resources. We need to understand and depict characteristics including: how precipitation is partitioned depending on its phase (Barnett et al., 2005; Carroll et al., 2020; Kirchner & Allen, 2020; Sprenger et al., 2022); how upstream and downstream components of the watershed are linked (Meixner et al., 2016); and how subsurface water is distributed to streamflow or evapotranspiration (ET) depending on the hydrologic condition and water age (Harman, 2019; Kirchner & Allen, 2020; Van der Velde et al., 2012).

Integrated hydrologic models consolidate our understanding of key watershed processes and have been widely, and often successfully, used to build our understanding of watershed processes and inform watershed management (Freeze & Harlan, 1969; Heppner & Loague, 2008; Maxwell & Kollet, 2008; Sulis et al., 2011). However, these hydrologic models are often tested primarily on integrated response variables such as streamflow. Integrated watershed models may reasonably reproduce the volumetric flux of water out of the watershed without correctly representing specific flow paths given substantial challenges with parameter non-uniqueness, raising questions about their value for prediction and projection (Beven & Freer, 2001). Conversely, conceptual "bucket" models have often used isotope measurements to determine which compartments contribute to streamflow, but they reflect only lumped watershed behavior and not spatially-discrete processes and so provide less detailed management information (Crouzet et al., 1970; Kirchner & Allen, 2020; Klaus & McDonnell, 2013).

Newly-developed dynamic-flux particle tracking models (Maxwell et al., 2019) provide novel information regarding the specific flowpaths packets of water take through a simulated watershed, accounting for temporally and spatially variable water fluxes. With advancements in high-performance computing, particle tracking tools are no longer limited to steady state models or models of limited scale and complexity (e.g., lysimter to research catchment scale, steady-state, or groundwater-only models; Danesh-Yazdi et al., 2018; Jones et al., 2006; Kim & Harman, 2022; Kollet & Maxwell, 2008; Pangle et al., 2017; Pollock, 2012; Wilusz et al., 2020). Dynamic-flux particle tracking in watershed-scale hydrologic models elucidates information about watershed behavior, including links between the source of both ground- and surface-water, watershed storage dynamics, and multi-scale watershed dynamics. This new capability also raises new challenges in visualizing these dynamics.

1.1. Hydrologic Connections and Sources: Key Tools for Planning

Water's flow into, through, and out of a watershed depends on the timing and intensity of rain and snowmelt, connections between mountain headwaters and valley groundwater, and groundwater mixing that drives distinct patterns of water release in time and space. Outstanding questions include: (a) Where and from what precipitation phase are streamflow and ET generated throughout the year?; (b) How old is water that exits the watershed as streamflow and ET?; and (c) Which characteristics determine how water from storage exits the watershed as streamflow or ET?

Previous work suggests snow is more efficient at producing streamflow than rain (Berghuijs et al., 2014; Davenport et al., 2020; Earman et al., 2006). Most recently, Carroll et al. (2020) and Sprenger et al. (2022) show that rain preferentially exits a headwater watershed as ET while snow contributes more to streamflow. However, many hydrologic analyses assume snow and rain behave similarly except for snow's storage capacity despite distinct conditions during precipitation and for different water fluxes and exit pathways.

Further, we need to investigate how watersheds are connected, how headwaters recharge valley groundwater and source streamflow and ET, and how these connections vary across space and time (Meixner et al., 2016; Schreiner-McGraw & Ajami, 2020, 2022). These connections may shift with changes in precipitation's spatial distribution, phase, and elevation. The elevation of infiltration may reveal important relationships between where precipitation falls and where it exits. We define elevation of infiltration simply as the elevation at which water, leaving as streamflow or evapotranspiration, infiltrated into the subsurface. These processes need to be appropriately represented in simulations to provide robust projections of watersheds' response to a shifting climate.

Exiting water's age and relationship to subsurface water storage in both the saturated and unsatured zones (hereafter storage) may also contain critical information on how the watershed will respond to a shifting climate. For example, old groundwater may have historically buffered streamflow and ET response to perturbations, but that buffering capacity could disappear as old reserves are drained. Whether storage will continue to provide resilience for both people and vegetation may depend on how and when water from specific sources exits storage. The response of a watershed to shifting precipitation might differ if the oldest water exits storage rather than if younger water exits storage. The former might suggest piston-type flow or fracture flow from old groundwater, both of which might support a resilient system in the short-term but result in a later state change that would provide a strong shock; the latter might suggest shallow interflow or fracture flow that would not occur as regularly but to which the system can adapt. Streamflow and ET may also draw from storage with distinct characteristics, in which case the resilience of human and natural systems may differ while still being strongly connected. Water age can also indicate large-scale watershed connections and groundwater replenishment rates that may shift with the climate. Conceptual storage-runoff modeling (Section 1.2.1) seeks to address these questions, but does not integrate complex catchment characteristics, geology, or flow feedbacks that may alter critical hydrologic connections (Danesh-Yazdi et al., 2018). We can account for these factors by specifically representing water's flow paths in a complex watershed to investigate how flow paths respond to a shifting climate.

Here, we use dynamic-flux particle tracking to investigate three critical questions and demonstrate this approaches' capabilities in analyzing details of hydrologic processes at the watershed scale for the first time. We further present a novel visualization approach, which we call water source wedges, to represent these complex processes across the watershed. First, we explore and illustrate the links between water's precipitation source phase and exit path to understand how snow and rain behave differently. We use the term “precipitation source phase” to distinguish between rain and snowmelt and the term “exit path” to distinguish between streamflow and ET. By inspecting these links we can both: (a) investigate whether and when snow and rain function differently in the watershed; and (b) test whether our simulations reliably represent this critical watershed function. Second, we examine the distributions of water source elevation separated by both precipitation source phase and exit path at two times to demonstrate how rain and snow connect to the exit paths depending on their source elevation and the time of year. Finally, we explore and depict the age of both exiting and storage water to understand: (a) the age of water exiting the system; and (b) the links between water age, storage characteristics, and exit processes. Such analyses will help us better represent watershed processes in simulations and predict the spatiotemporal variability of streamflow, ET, and storage as snowfall shifts to rain in a warmer climate. These analyses could be compared with isotopic and chemical measures sensitive to precipitation source phase, initial elevation of precipitation or infiltration, or water age to constrain watershed simulations and ensure they accurately represent water's flow paths and provide robust projections.

1.2. Previous Advances in Watershed Modeling

Watershed modeling encompasses a broad variety of approaches, including conceptual storage-runoff models that lack spatially-explicit connections and distributed (spatially-discretized) flow models that lack specific techniques to track flow paths among them. Our work seeks to bridge this gap by incorporating the awareness of sources and residence times of conceptual models with spatially-explicit connections in distributed flow models, following previous attempts with different approaches (Glaser et al., 2021; Jing et al., 2021; Weill et al., 2019).

1.2.1. Isotopes and Conceptual Storage-Runoff Modeling

Several techniques use isotope measurements to assess the residence times, sources and storage of water in watersheds. Isotope-based hydrograph separations (IHS) used tritium measurements in rain, groundwater, and streamflow (Crouzet et al., 1970; for a recent review, see Klaus & McDonnell, 2013) to show that stored, pre-event water dominated the storm hydrograph in most natural, humid systems (Sklash et al., 1976). This contrasts with previous hypotheses that event flow was generated largely by overland flow (Dunne & Black, 1970). Newer approaches link specific water sources with water outputs and explicitly track the time that water spends in a watershed using stable and radioactive isotopes as well as man-made environmental or introduced tracers (Benettin et al., 2022).

STorage Outflow Probability (STOP) functions (Van der Velde et al., 2012) or StorAge Selection (SAS) functions (Harman, 2019) extend the interpretation of isotope hydrographs beyond pre-defined age distributions. STOP/SAS functions describe water movement from storage to streamflow (or ET) relative to the residence times of water in storage and emphasize the continuum of flow paths in a natural watershed. This framework incorporates the dynamic behavior of watersheds into storage-discharge relationships. While STOP/SAS describes the fate of storage water, isotope-based endmember splitting (Kirchner & Allen, 2020) describes the fate of precipitation. This distinction is particularly important in snow-dominated watersheds that are sensitive to climate change where precipitation phase determines flux rates (rain vs. snowmelt) and watershed response.

These techniques lump watershed behavior and lack specific information on spatial connections that may be critical for managing water resources in larger, heterogeneous watersheds. In addition, these models derive predictive ability solely from historic isotope observations; therefore, their ability to predict watershed behavior in a changing climate is uncertain. However, these approaches are computationally tractable while watershed-scale modeling of flows and transport of (isotope) tracers has historically been limited by the computational demands of a model with sufficient spatial and temporal resolution to realistically simulate heterogeneous and time-variable behavior. Further, distributed physics-based models struggle with the challenge of equifinality (Beven & Freer, 2001).

1.2.2. Integrated Watershed Modeling and Particle Tracking

Integrated watershed models provide an alternate approach to assess watershed flow processes. These models explicity represent the volumetric flux of water over space and time, and therefore include appropriate spatiotemporal connections for realistic simulation (Brunner & Simmons, 2012; Freeze & Harlan, 1969; Kollet & Maxwell, 2006). Such simulations have been widely used to understand hydrology from hillslopes to nations (Condon & Maxwell, 2019; Maxwell & Kollet, 2008) and for management of water resources (Heppner & Loague, 2008; Maxwell & Condon, 2016; Maxwell & Kollet, 2008; Sulis et al., 2011) and potential contaminants (Loague et al., 2005; Siirila-Woodburn et al., 2018; Sudicky et al., 2008; Visser et al., 2012).

However, integrated watershed models do not directly investigate spatial connections because they represent only the volumetric flux of water in an Eulerian framework that cannot distinguish individual flow paths across model cells. Lagrangian particle-tracking techniques use velocity fields from physics-based groundwater or integrated watershed models to track specific hydrologic connections at much higher resolution (e.g., Engdahl & Maxwell, 2015; Kollet & Maxwell, 2008; Pollock, 2012; Visser et al., 2009) and have been widely used to determine flow paths for contaminant analyses (Siirila-Woodburn, Fernàndez-Garcia, & Sanchez-Vila, 2015; Siirila-Woodburn, Sanchez-Vila, & Fernàndez-Garcia, 2015; Zhang et al., 2013). However, classic particle-tracking techniques use relatively simple particle insertion schemes and/or follow water parcels that do not interact with surface water and other land-surface processes. These approaches cannot properly represent the fluxes of water through the system because they do not dynamically link particles with water entering the watershed as precipitation and exiting as streamflow or ET. Therefore, they do not illuminate important spatio-temporal dynamics of watershed connectivity or separate precipitation input phase, a critical consideration as outlined above. Recent work has sought to more dynamically represent the spatio-temporal dynamics of water sources and travel times based on tracking of fluxes or hydraulic mixing cells, sometimes in combination with explicit particle representations for deeper subsurface flow (Glaser et al., 2021; Jing et al., 2021; Li et al., 2017). Another recent approach uses a depth-integrated hydrologic simulator to investigate transit and residence time distributions (Weill et al., 2019). These approaches can provide valuable information about water's flow paths, but require assumptions about mixing or distributions with depth.

The dynamic-flux particle tracking approach shown here provides age- and source-dependent fluxes that can be compared with tracer measurements to better parameterize model behavior based on detailed flow simulations. It represents explicit flow of water through the subsurface, including variability with depth and makes no specific mixing assumptions, though at increased computational cost relative to other approaches. If integrated watershed models and particle tracking techniques are well-parameterized, then changing climate forcings in such simulations could provide valuable insight on watershed behavior change in the future and, along with other approaches, inform more sustainable water resource management.

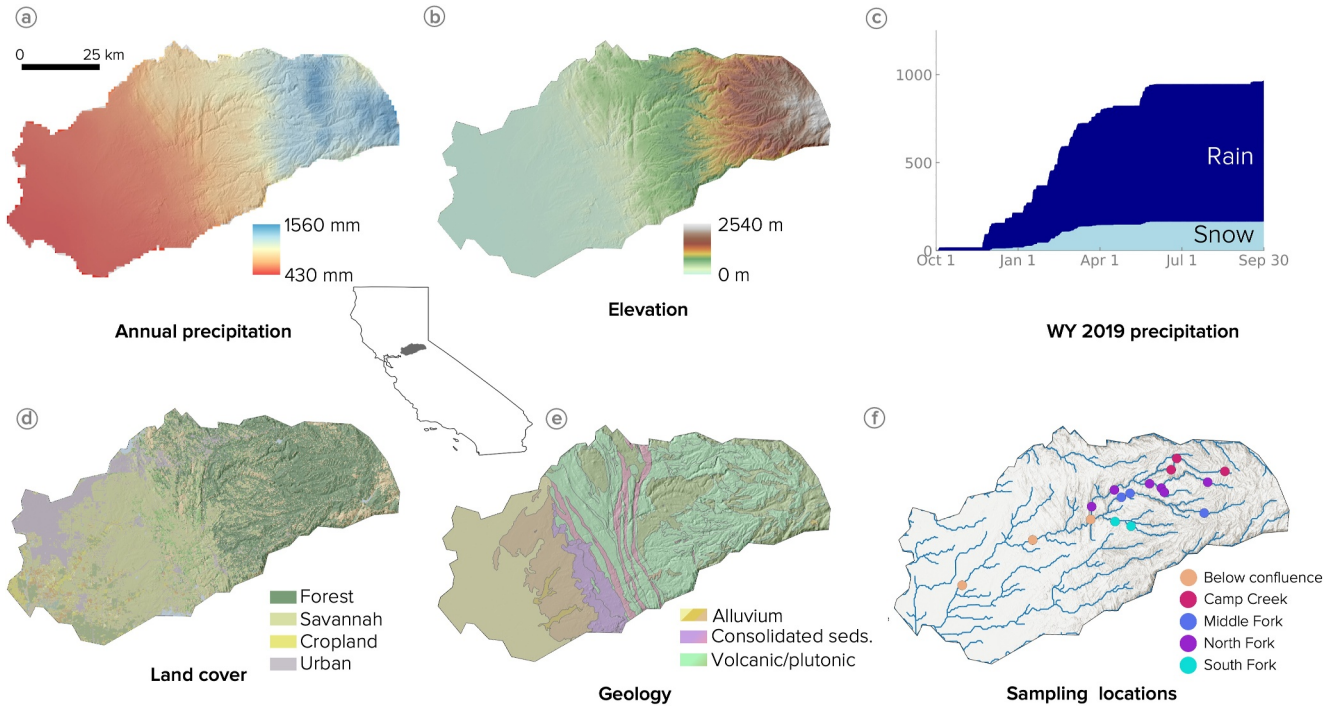

Figure 1. Watershed, climatic characteristics, and community-led sampling locations of the Cosumnes Watershed, the model domain for which is shown in the inset map of California in dark gray. Average annual precipitation (a) totals range from 430 mm in the near-sea-level lowlands and up to 1,560 mm at elevations above 2,350 m (b). Watershed-average cumulative precipitation from water year 2019 (c) used in the simulation is mostly rain, shown in dark blue, but with ~20% starting as snow shown in light blue. The land cover (d) is largely forest in the upper watershed and savannah in the lower watershed, with substantial urban and cropland areas in the lower watershed as well. The watershed is underlain by alluvial packages in the lower part, by low-permeability cross-cutting consolidated marine sediments in the middle of the watershed, and volcanic and plutonic packages in the upper part of the watershed (e). The American River Conservancy has a sampling program in the watershed (f), and spatially-limited analyses here are shown at those points, though comparisons with those measurements are not yet complete.

2. Methods

We present a novel watershed-scale analysis using EcoSLIM, a new particle tracking tool that simulates the full spatio-temporal dynamics of water particles (Maxwell et al., 2019), to demonstrate this class of codes' utility for hydrologic analysis. The spatially explicit flow field, interpolated from velocity vectors from the integrated hydrologic model ParFlow, enables spatial characterization, while appropriate temporal dynamics are provided by dynamically adding and removing particles. Further, by tagging particles based on their precipitation source phase, exit pathway, input and exit location, age, and other factors (e.g., flow path length, time in saturated zone) we can investigate key dynamics across space and time. With EcoSLIM, we simulated the detailed flow paths of water from Sierra Nevada snowpack to the Central Valley in the Cosumnes watershed (Section 2.1) to better understand hydrologic connections from headwaters to groundwater. We developed several tools to run EcoSLIM at this large scale (~10^4 km^2) and to analyze large numbers of particles (~10^8) across space and time to advance our hydrologic understanding via novel analyses described in Sections 2.3 and 2.4. We further developed a novel approach to visualize the EcoSLIM outputs to explore the source location, precipitation phase, and age of both streamflow and ET across the watershed (Section 2.4.1).

2.1. Cosumnes River Watershed

The Cosumnes River Watershed (Figure 1) covers 3,300 km^2 from the lower Sierra Nevada (~2,350 m elevation), where 1,500 mm of precipitation falls as snow annually, to the Central Valley (near 0 m elevation), where groundwater is pumped for irrigation and annual precipitation is only 600 mm. The precipitation has strong seasonal variability, virtually all occurring in the winter, and an inter-annual coefficient of variation around 0.35 (Dettinger et al., 2011). The watershed's geology ranges from upland plutonic rocks and volcanic flows to unconsolidated sandstone and Central Valley alluvium; these are separated by cross-cutting shales and sandstones. The land cover varies strongly with elevation, from fir, pine, and incense cedar conifers in the upper

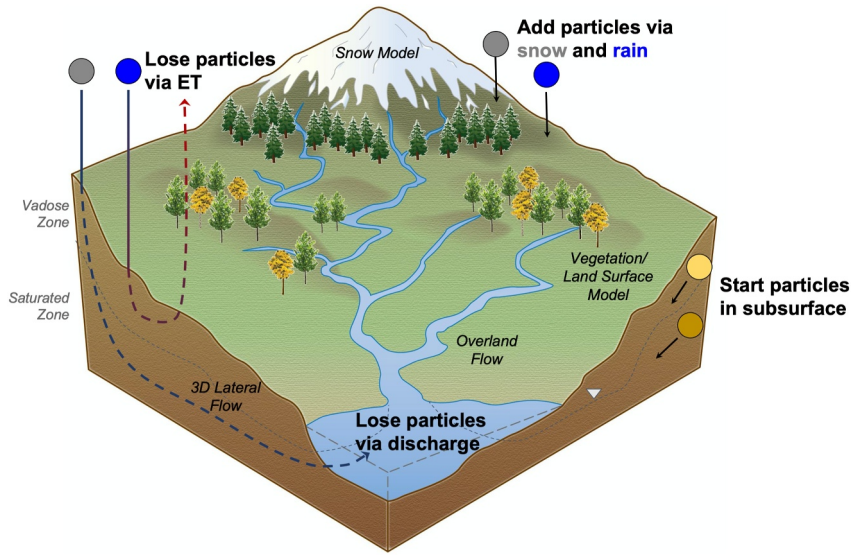

Figure 2. Conceptual diagram for the Parflow-CLM and EcoSLIM coupling, showing both ParFlow's integrated watershed model of subsurface flow and surface processes and the dynamic fluxing of particles through the system using EcoSLIM.

watershed to oak savannah lower in the watershed. Pastures and cultivated crops dominate in the Central Valley. The Cosumnes Watershed is the focus of integrated headwaters-to-groundwater research seeking to understand the impacts of climate change on California water resources (Maina et al., 2020; Maina & Siirila-Woodburn, 2019).

2.2. Dynamic-Flux Particle Tracking in a Fully-Integrated Surface-Water/Groundwater Model

2.2.1. ParFlow-CLM

ParFlow-CLM is a fully-integrated surface-water/groundwater model that is coupled with the Community Land Model (CLM) for surface and ecologic processes (Kollet & Maxwell, 2006; Maxwell, 2013; Maxwell & Miller, 2005) (Figure 2). It solves the Richards' equation for unsaturated and saturated flow throughout a subsurface domain and simultaneously solves shallow water flow equations on the surface. Vertical water and energy fluxes at the land surface and exchanges with the lower atmosphere are handled by a version of the Community Land Model similar to version 3.5 (Dai et al., 2003; Maxwell & Miller, 2005). ParFlow-CLM was developed to run on computational platforms ranging from laptops to supercomputers, and scales well up to tens of thousands of processors (Kollet et al., 2010).

We use a previously developed ParFlow-CLM simulation of the Cosumnes Watershed (Maina et al., 2020) shown to reasonably represent watershed behavior based on both in-situ and remotely sensed hydrologic measures (Maina et al., 2020). That simulation shows a mean absolute error (MAE) in river stage of ∼0.6 m at three river gauges, an MAE of ∼1.7 m and mean absolute percent error (MAPE) of ∼2.5% for four groundwater wells over the 3 years of simulation. Further, the simulation has an MAE of only ∼3 mm and watershed-average temporal correlation of ∼0.97 with the SNODAS data set (National Operational Hydrologic Remote Sensing Center, 2004), and watershed-average temporal correlations of 0.94 with the SMAP soil moisture estimates (Reichle et al., 2017) and 0.6 with METRIC ET estimates (Allen et al., 2007). More details are available in Maina et al. (2020). We analyze water year 2019 (1 October 2018–30 September 2019, hereafter WY2019), the final year of that simulation, which represents an average-to-wet water year. The model is forced hourly by the NLDAS-2 product for meteorological variables: precipitation, temperature, short- and long-wave radiation, two-dimensional wind speed, atmospheric pressure, and relative humidity. The model is spatially discretized by cells that are 200 m in each horizontal direction, and 8 vertical layers that range from 10 cm deep in the soil to 30 m deep in the subsurface, creating an 80 m thick model on a terrain-following grid. In the model, 1.3 million active cells compose the approximately 7,000 km^2 model area, which includes the Cosumnes Watershed and surrounding areas to set boundary conditions based on observed river stages. The model requires approximately 48

wall hours of compute time on 320 Intel Haswell processors for a single year of simulation. Simulations were performed on the National Energy Research Scientific Computer Center (NERSC) supercomputer Cori.

Watershed topography was derived from the USGS 3D Elevation Program, geology from California geological maps (Geologic Map of California, 2015; Jennings et al., 1977), and land cover from the 2011 NLCD land cover data set (Homer et al., 2015). Watershed and geological characteristics were translated to model parameters based on literature values. Boundary conditions include a no-flow boundary condition along the bottom of the watershed and both no-flow and temporally varying constant head values for the upper watershed and surrounding rivers, respectively (Maina et al., 2020).

2.2.2. EcoSLIM

EcoSLIM is a dynamic-flux particle tracking tool fully compatible with ParFlow-CLM or other integrated hydrologic models with similar output (Maxwell et al., 2019) (Figure 2) and was adapted from the SLIM and SLIM-fast particle tracking tools (Kollet & Maxwell, 2008; Maxwell & Kastenberg, 1999; Maxwell et al., 2007). Recent work has been developing EcoSLIM to allow applications on GPUs at very large scale (Yang et al., 2021, 2022, 2023). We describe EcoSLIM as having a "dynamic-flux" because particles enter and exit the system dynamically, unlike in traditional particle-tracking approaches. Particles are added to the subsurface simulation based on infiltration from the surface after snowmelt or rainfall, and removed from the subsurface simulation through both streamflow and evapotranspiration (ET). Thus, the model faithfully represents watershed dynamics, in which water dynamically fluxes through. Particles advect according to an interpolated velocity field from the ParFlow simulation, which is computed before EcoSLIM is applied. The EcoSLIM simulation requires time-varying three-dimensional flow, saturation, and surface-subsurface fluxes for each model cell, a time-varying CLM indicator for rain or snow for each of 160,000 surface cells, and a static porosity characteristic. Hard drive requirements for 1 year of simulation are approximately 1 TB of ParFlow simulation data and approximately 500 GB for EcoSLIM simulation data.

New particles are added each 1-hr simulation timestep if there is a net flux of water into the subsurface domain representing precipitation, snowmelt, or surface water infiltration. Particles are tagged with important *characteristics* as they enter the subsurface, including: mass, time and location of entry, and precipitation source phase (snow, rain, or initial groundwater). Each particles' age and flow path length characteristic starts at 0 and is updated as it flows through the system. As particles exit the model, additional characteristics are recorded, including exit pathway (streamflow or ET), and location and time of exit; the age and flow path length are also finalized. Particle mass depends on the infiltration mass and so varies across particles. Particles are tagged as snow or rain depending on whether there is snow-water equivalent in the CLM cell—thus both rain and irrigation are tagged as rain since there is generally no snow-water equivalent in irrigated cells. Particles are removed by ET depending on the particle mass and the water mass evapotranspired through CLM.

The EcoSLIM simulation was spun up and run using the WY2019 ParFlow simulation. Initially, one particle was placed in each active model cell to represent the water initially present in the domain. These particles are considered initial groundwater, but are not included in water source and age distributions because—after a 35 years spinup period—they represent a minimal fraction of the water existing in the watershed (<1%). A single particle was added in each cell for each hour in which infiltration occurred into that cell, with particle mass equal to the infiltration mass. The model ran as discussed above for 35 sequential years, repeatedly driven by the velocities and infiltration masses from the WY2019 ParFlow simulation, with particles exiting by both streamflow and ET. We considered the spinup complete when the average particle age over the domain changed less than 0.2 years between simulation years (~0.5% of the simulation time), as shown in Figure S1 in Supporting Information S1. We accepted this rough convergence after 35 simulation years due to the large size of the model—simulations required ~48 hr on 32 Haswell cores for each year of spinup with ~700 million particles, nearing the memory limits of available resources. While future work could achieve better convergence, this level of convergence demonstrates the capabilities and techniques of EcoSLIM.

2.2.3. Adapting for Watershed-Scale Application

To our knowledge, our work represents the largest applications of advanced dynamic-flux particle tracking in a single watershed to date, with ~700 million active particles and billions of particles overall. We adapted EcoSLIM in two ways to enable application at this scale: turning off diffusion to avoid generating trillions of random

numbers per simulation year, and modifying the output code to reduce computation time. These approaches each provided ~2x speedup resulting in a model speedup of ~4x. More details can be found in Text S1 in Supporting Information S1. The modified code is available on GitHub: https://github.com/pjdf/EcoSLIM.

2.3. Particle Analysis

We developed several new techniques to analyze EcoSLIM outputs in a large watershed model and address questions regarding the precipitation source phase and elevation of streamflow and ET, the spatiotemporal variability of water age in streamflow and ET, and the storage selection behavior. These analyses focus on important hydrologic processes represented by particle movement and enable future comparison with observations of tracers reflecting the source, precipitation phase, and ages of water in the watershed.

2.3.1. Selecting Exit Particles Based on Precipitation Source Phase and Exit Path, Localized in Space and Time

We characterize the spatiotemporal variation of both streamflow and ET in terms of water age and precipitation source phase. We select the particles exiting each of 17 (nested) subwatersheds for each simulation hour. These watersheds represent stream monitoring locations regularly sampled for hydrologic and geochemical characteristics by a local non-profit, the American River Conservancy, to enable future model-data comparisons beyond this study's scope. We summarize these fluxes by the volume of water represented by particles leaving the system during each timestep through each exit path from each subwatershed; we aggregate these both by precipitation source phase and by age. These steps are detailed in Text S2 in Supporting Information S1. After this processing, we can investigate detailed hydrologic function and flow paths in ParFlow and analyze how these processes depend on local characteristics and conditions.

2.3.2. Selecting Particles in Storage Across Space and Time

We investigate the age of both streamflow and ET relative to that of the water in storage using age-ranked storage-selection (SAS) functions (Rinaldo et al., 2015). These functions compare the distributions of the age of water exiting the system with that of the water in storage to determine whether the water exiting the watershed is effectively randomly sampled from storage (as in a well-mixed system) or has age characteristics that are distinctly different from storage. This helps us understand the fundamental watershed behavior and the dynamics of the aggregated effects of all flow paths water takes through the subsurface. For these analyses, we select particles from *storage* across space and time following the first three steps in Text S2 in Supporting Information S1. Note that this selects all particles in a vertical column below the subbasin surface shape, and therefore does not discriminate if particles are part of a local flow system or not. Such an analysis is possible but beyond this study's scope.

We then compare particle age distributions of exit fluxes (Section 2.3.1) and storage at two times during the year to explore the variation in storage-selection behavior during distinct hydrologic conditions and distinguish different precipitation source phases and exit paths. Similar analyses could be done for water input elevation or other characteristics.

2.4. Hydrologic Analysis

We focus on three key characteristics of watershed processes: precipitation source phase, source elevation, and water age. Particle tracking results were analyzed in three distinct ways: novel subwatershed-scale cumulative time-series, simultaneously illustrating the temporal evolution of the precipitation phases contributing to ET and streamflow, as well as their age distribution (Section 2.4.1), cumulative distribution functions of water source elevation and age (Section 2.4.2) and storage selection behavior (Section 2.4.3).

2.4.1. Analyses of the Spatiotemporal Variation of Water Flux Sources and Ages

We develop a novel graphical approach to investigate when, where, and from what source both streamflow and ET are generated which we call "water partitioning wedges." As shown in the Figure 3 inset, these wedges show cumulative time-series of both streamflow (blue colors, downward) and ET (red colors, upward) for snow in light shades and rain in dark shades. We plot these in map form at subbasin outlets as a comprehensive approach to

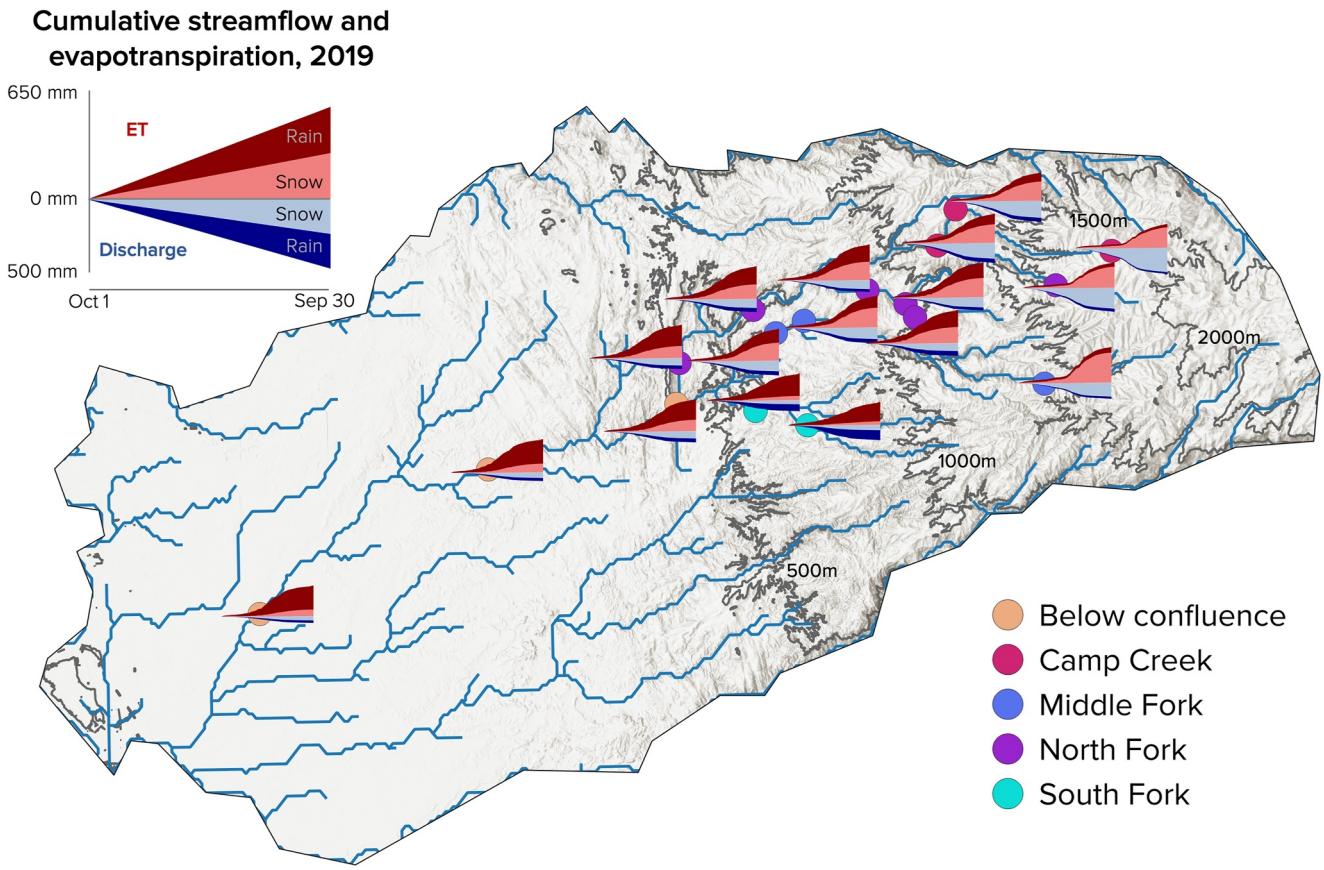

Figure 3. Simulated cumulative streamflow and evapotranspiration for water year 2019 in the Cosumnes watershed distinguished by precipitation phase. Cumulative curves are located at each of 17 locations sampled by volunteers in the American River Conservancy. Cumulative streamflow in blue goes down from the 0 line and evapotranspiration in red goes up from the 0 line, with the water that originated as snow in the light blue and light red and the water that originated as rain in dark blue and dark red. Across the watershed snow preferentially leads to streamflow, while rain leads to evapotranspiration at the larger scale but is more evenly split between streamflow and evapotranspiration in the headwaters. The higher elevation of the watershed is dominated by snow input and by streamflow output, while the lower elevation part of the watershed is dominated by rain input and evapotranspiration output. There is also a distinct temporal difference in the upper and lower watershed, with faster rises in evapotranspiration and especially streamflow because of the snowmelt period. The South Fork of the Cosumnes (in aqua) shows distinct behavior from other headwaters because its lower elevation means it is rain dominated—here, most of the snow still leads to streamflow but a majority of the streamflow and evapotranspiration both come from rain. A high-resolution version of this figure is available for closer inspection as Figure S3.

visually interpret spatio-temporal water partitioning across the watershed. We inspect the cascade of these distinct water source, age, and exit characteristics downstream across the stream network as more and different headwaters are integrated into the system. Figure 3 shows curves for the 17 aforementioned subwatersheds, spanning from headwaters to valley, but any set of subbasins could be selected.

Similarly, we investigate the age of both streamflow and ET across the watershed (Figure 5). In this case, the cumulative time-series of streamflow and ET illustrate the proportions of water in four age bins: (a) younger than 5 days; (b) within the water year; (c) less than 5 years old; and (d) more than 5 years old. Bin boundaries can be adapted to the watershed under consideration.

2.4.2. Analyses of Water Source Elevations and Ages With Cumulative Distribution Functions

We investigate how source elevation varies across time depending on the precipitation source phase and exit path by analyzing cumulative distribution functions (CDFs) of infiltration elevation. We plot the CDF of the infiltration elevation for particles that exited the watershed during May 2019 and September 2019 (Figure 4). These months provide a strong contrast in flow conditions to elucidate the distinct behavior of the watershed across time. May is a relatively high-flow period, after peak snowmelt but before the summer dry season, while September is a low-flow period after many faster flow paths have emptied and so represents the system's longer flow paths. CDFs

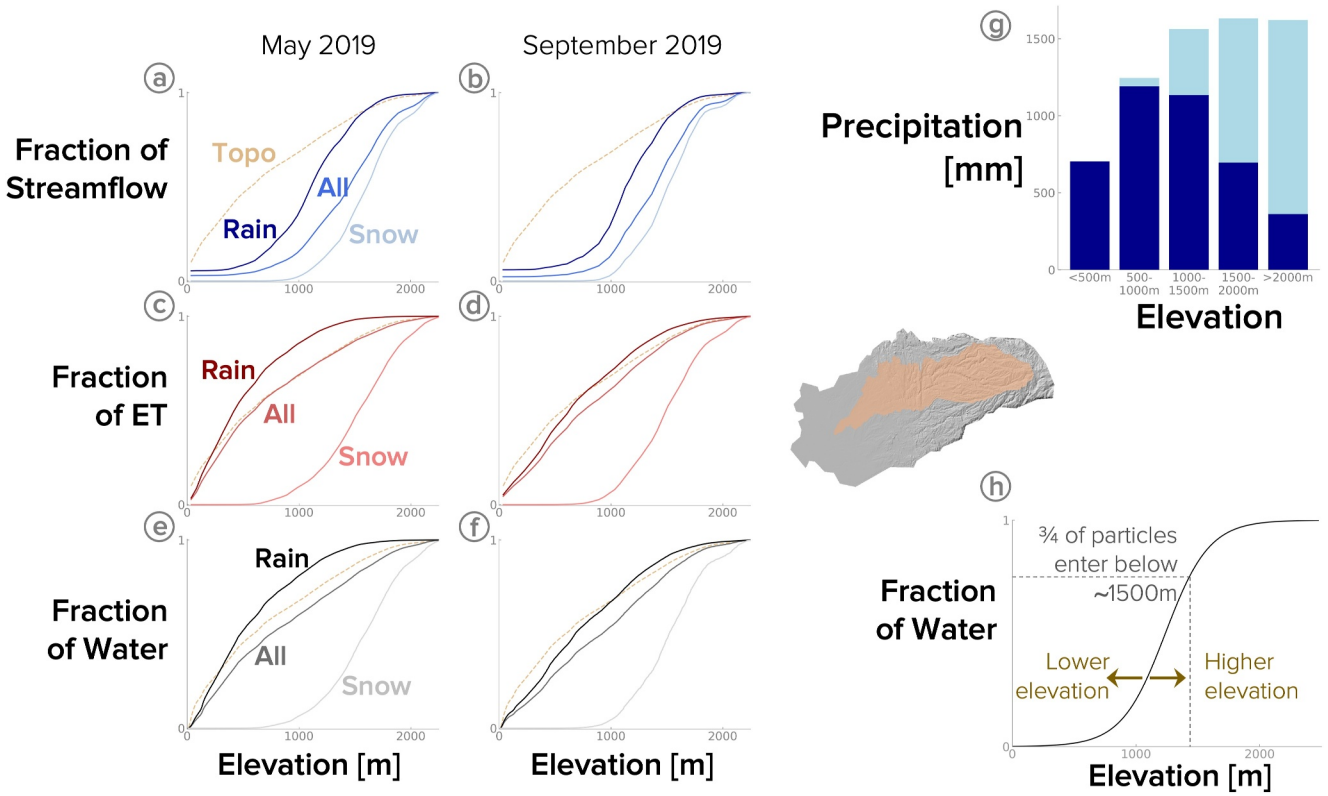

Figure 4. Cumulative distribution curves of the source elevation of simulated streamflow (a, b) in blue, evapotranspiration (c, d) in red, and the total water lost (streamflow and evapotranspiration; e, f) in gray for May 2019 (a, c, e) and September 2019 (b, d, f) for the watershed defined by the river at Mahon Ranch, shown in tan on the shaded relief map at the right. Darker colors indicate water that originated as rain, the lightest color indicates water that originated as snow, and the middle color indicates the sum of the two. The dashed brown line shows the cumulative distribution function of elevation in the same watershed. Average precipitation amounts and their origin phase are shown in the bar graph (g) for 500 m elevation bands with water starting as rain in dark blue and as snow in light blue, showing the dominance of snow in the upper watershed and rain in the lower watershed. Note that the total area above 1,500 m is relatively small, as seen in the cumulative distribution of elevation. The explainer curve (h) shows how to read the plot and that if the line shifts left it means more water starts at lower elevation, and if it shifts right more water starts at higher elevation.

are built separately for the water that exits as streamflow and that which exits as ET, as well as for water that falls as rain and that which falls as snow. These are plotted side-by-side to easily compare across the two time periods, exit paths, and precipitation source phases. In addition, we plot the CDF of land surface elevation (brown dotted lines labeled "Topo"). This demonstrates the distribution from a spatially homogeneous precipitation in which water exited at the same elevation at which it enters.

We perform a similar analysis for water age, plotting the cumulative age distributions of all water exiting the watershed in both May and September 2019 (Figure 6). We further plot the age distributions for each precipitation source phase as well as for each exit path.

2.4.3. Analyses of the Selection of Streamflow and Evapotranspiration Water From Storage

We investigate the simulated storage-selection dynamics by building age-ranked storage-selection curves. To do so, we calculate the cumulative age distributions of all particles in storage in the middle of both May 2019 and September 2019 with the same age bins used to calculate the cumulative age distributions for exiting particles in Section 2.4.2. Note that this determines distinct age distributions of the particles in storage across seasons, distinct from Wilusz et al. (2020). We then plot the CDF of storage particle ages on the *x*-axis against the CDF of *exiting* particle ages for that month on the *y*-axis. That is, we show the relationship between water in storage and exiting storage for a set of water age ranges to determine the system dynamics and any preferential behavior of specific water ages. If data plots along the 1:1 line, then the water exiting the system has the same age distribution as the water in storage. If the slope of the plotted data is steeper than 45° (the 1:1 line), then water in that age range is

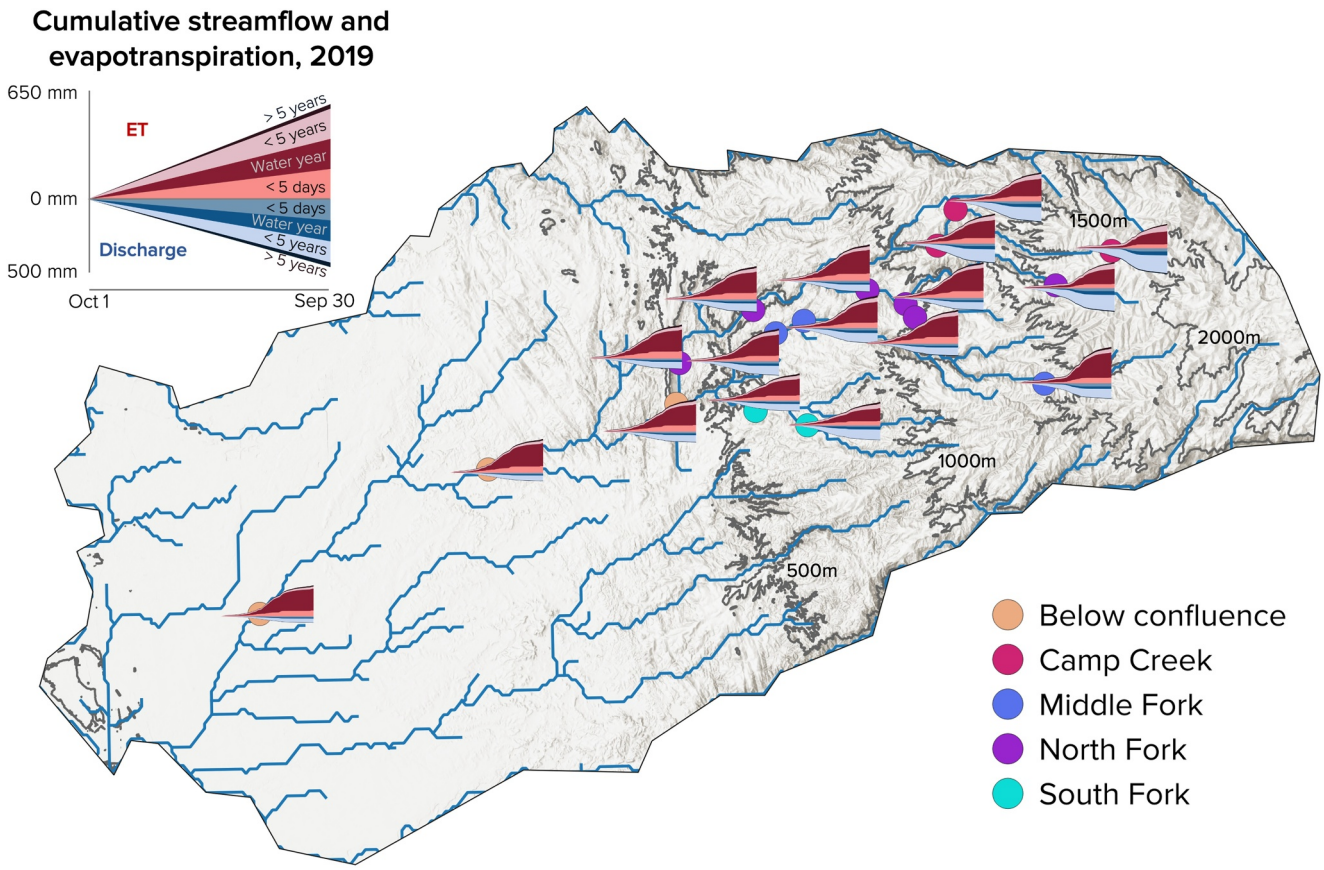

Figure 5. Simulated cumulative streamflow and evapotranspiration for water year 2019 in the Cosumnes watershed distinguished by water age. Cumulative curves are located at each of 17 locations sampled by volunteers in the American River Conservancy. Cumulative streamflow in blue goes down from the 0 line and evapotranspiration in red goes up from the 0 line, with the colors representing water age as shown in the key in the upper left. Streamflow is dominated by water that fell before the current water year but within the last five years, though there is also a substantial portion that entered the system very recently (less than 5 days old) in the upper watershed. Evapotranspiration, in contrast, is dominated by water that fell within the water year, with a significant fraction that fell within five days in the lower watershed and a larger fraction that fell before the current water year but within five years in the upper watershed. A high-resolution version of this figure is available for closer inspection as Figure S4.

more likely to exit the system compared with other storage water. Conversely, if the line is less steep than 45°, water in that age range preferentially remains in storage compared to other storage water.

Storage selection functions are built separately for each water exit path and for all water which exits. In addition, storage selection curves are built separately for water from each precipitation source phase as well as for the total infiltration. Our figures represent the *fractional* age-ranked storage selection functions (fSAS) that are scaled to total streamflow and total storage volume at each time (Van der Velde et al., 2012). *Fractional* age-ranked storage selection functions illustrate watershed behavior with respect to the youngest and oldest water in storage, so their shape is less sensitive to the relationship between storage volume and water exit rate and more easily comparable across different times. In contrast, ranked storage selection functions (rSAS; Harman, 2019) require arbitrary scaling of both axes depending on streamflow and storage conditions; we present fSAS functions to directly compare watershed behavior at different times.

3. Results

3.1. Spatiotemporal Variability in the Contributions of Rain and Snow to Streamflow and Evapotranspiration

The simulated precipitation source phase of streamflow and evapotranspiration varies across the watershed in space and time as seen in the water partitioning wedges for each sampling point in 2019 (Figure 3). Each cumulative hydrograph illustrates the precipitation phase (rain in darker colors, snow in lighter colors), the partitioning

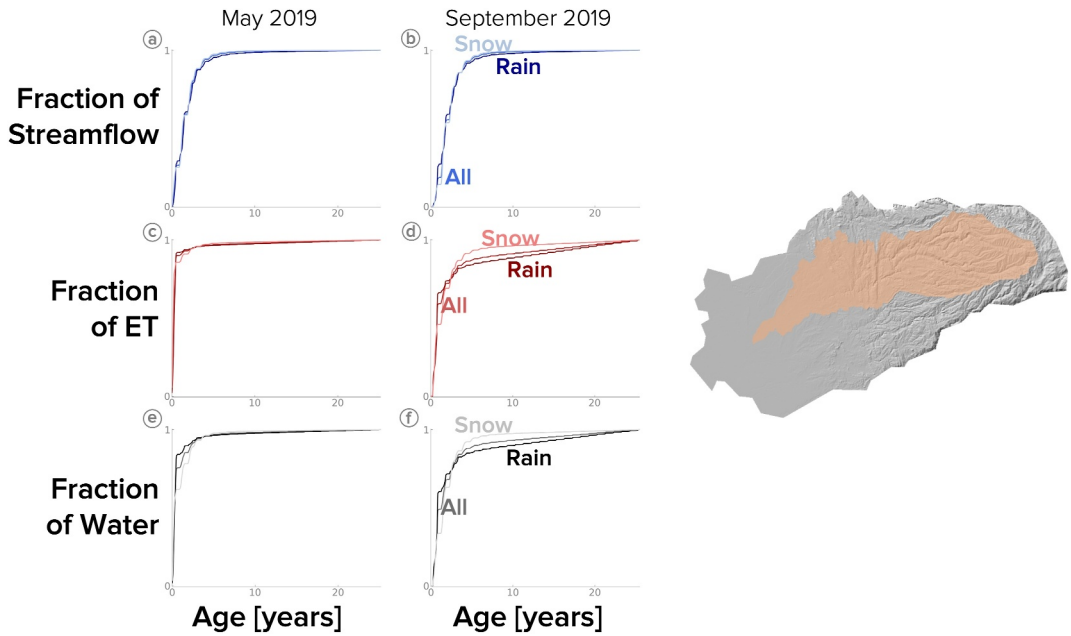

Figure 6. Cumulative distribution curves of the age of simulated streamflow (a, b) in blue, evapotranspiration (c, d) in red, and the total water lost (streamflow and evapotranspiration; e, f) in gray for May 2019 (a, c, e) and September 2019 (b, d, f) for the watershed defined by the river at Mahon Ranch, shown in tan on the shaded relief map at the right. Darker colors indicate water that originated as rain, the lightest color indicates water that originated as snow, and the middle color indicates the sum of the two. The September streamflow is slightly older than the May streamflow, and shows more differentiation between the snow and rain sources, with somewhat more water from the 1–3 years age range coming out and then slightly less in the 3–10 years age range. Evapotranspiration shows a more significant shift to older water in September and shows a clearer separation between rain and snow, though with the same basic pattern. The same pattern is observed in the total exited water as well, matching the rain more closely because the system is rain-dominated.

between streamflow (bottom, blue) and evapotranspiration (top, red), and the timing of each of the fluxes. Higher elevations see most of their water come in as snow and, in the highest elevations, most of that water leaves as streamflow (light blue). The lower watershed is dominated by rain input and evapotranspiration output (dark red). In this watershed simulation, snow preferentially exits as streamflow while rain preferentially exits as evapotranspiration at the watershed scale. However, rain partitions more evenly between streamflow and evapotranspiration (ET) in the headwaters.

In the upper headwaters of Camp Creek, the North Fork, and Middle Fork, nearly all water that exits the model system starts as snow. In the more northerly Camp Creek and North Fork, the snow splits nearly equally between streamflow and ET, while in the more southerly Middle Fork more snow goes to ET. The small quantities of rain in these headwaters also split relatively evenly between streamflow and ET.

The headwaters also show distinct seasonal streamflow trends in the model: a gentle slope indicates small streamflow from the water year's start to snowmelt, then a steep increase during snowmelt indicates a short period of high streamflow, and finally a low slope after snowmelt indicates the near-cessation of streamflow. In contrast, simulated ET increases imperceptibly early in the water year. After snowmelt, ET increases steeply as water and energy become available, before gradually slowing over the course of the summer, contrasting with streamflow's relatively sudden stop.

The South Fork of the Cosumnes shows behavior distinct from other headwaters in the simulation because it is at lower elevation and thus rain-dominated. Here, most snow leads to streamflow but the majority of both streamflow and ET comes from rain. Streamflow here is dominated by pulses from individual storms rather than distinct seasonal trends. ET increases gradually early in the year, indicating low energy fluxes. This headwater zone is water-limited late in the year, minimizing ET and turning the streams ephemeral as seen in both field observations and the simulation.

In contrast with the headwaters, more water leaves the whole watershed simulation as ET than streamflow. This is seen in the water partitioning wedges at Mahon Ranch, the lowest sampling point in Figure 3. Mahon Ranch's simulated streamflow consists nearly evenly of rain and snow despite ~80% of watershed-wide precipitation falling as rain, while ET mostly fell as rain. About 15% (160 mm) of this "rain" may come from Central Valley irrigation, which is added for simulation fidelity and tagged as rain since snow-water equivalent during irrigation is 0. However, ET's increased influence can also be seen above the irrigation zone at sampling points near the confluence of the North, Middle, and South Forks. For example, at the North Fork above Sand Ridge Bridge (site 9 in Figure S2 in Supporting Information S1), 57% of total input is rain and 76% of exiting water is ET, while at Mahon Ranch, 72% of precipitation comes in as rain and 83% leaves as ET. The whole watershed also behaves differently from the upper headwaters, with gentler rises in streamflow and ET than even the South Fork headwaters because the watershed behaves as a low-pass filter smoothing out effects from many subwatersheds.

We can follow the cascading influence of the different water input and exit phases through the watershed in the model. Rain from the North and Middle Forks must preferentially contribute to ET as moving down the network streamflow remains snow-dominated, but the percentage of ET coming from rain slowly increases. This cascading behavior can alternately be seen by investigating water exit and precipitation phases across elevation at different times of year (Figure 4). Modeled streamflow originates mostly from high elevations. Nearly 85% of streamflow at Mahon Ranch in May originates above 1,000 m elevation, only a third of that subwatershed's area. In September the streamflow source moves slightly higher, with 88% originating above 1,000 m elevation. The latter occurs both because the average infiltration elevation of streamflow from snow moves from 1,625 m in May down to 1,520 m in September, and because the average infiltration elevation of streamflow from rain moves from 1,125 m in May to up to 1,150 m in September. In both periods more than 95% of the streamflow that fell as snow has an infiltration elevation above 1,000 m.

In contrast, May ET seems to be sourced from water that infiltrated evenly across the watershed in the model. The ET total consists of both rain-sourced ET that infiltrated at lower elevations and snow-sourced ET that infiltrated at higher elevations; the mass-normalized combination of the two signals lays nearly on top of the watershed elevation curve. ET in September is sourced from slightly higher elevations, with lateral flow contributing extra water to lower elevations and possible water limitation in the lowest elevations. The rain and overall ET curves are similar, showing that rain is the dominant source of ET, particularly in September. The entire watershed simulation's hydrology is dominated by ET as seen by the strong similarity of the overall water source curves to those of ET, both in May and September. This is consistent with the much larger ET volumes in the Mahon Ranch water partitioning wedges.

3.2. Spatiotemporal Variability in Streamflow and Evapotranspiration Water Age

In the Cosumnes simulation, ET is generally younger than streamflow, though the oldest water leaving the watershed (25 years old) leaves as ET (Figure 5). ET is dominated by water that fell within the current water year (90%) whereas most streamflow fell before the current water year but within the last five years (65%). The ages of streamflow and ET differ most in the headwaters. In Camp Creek and the North Fork, more than 70% of streamflow fell before the current water year while more than 70% of ET fell within the current water year. In these headwaters, a substantial fraction of ET fell before the current water year but less than 5 years ago, while watershed-wide only about 10% of ET fell before the current water year. In contrast, streamflow includes similar fractions of water in each age bin between the headwaters and the whole watershed, suggesting that the lower watershed contributes only a small amount to streamflow.

The age distributions of simulated streamflow and ET change differently going from headwaters to downstream, similar to downstream changes in the precipitation source phase (Section 3.1). Watershed-wide, streamflow is contributed by the upper watershed, as noted above and seen in reduced area-normalized streamflow volumes. Thus, streamflow has similar age fractions throughout the watershed. In contrast, the fraction of older ET is much larger in the highest elevations than at watershed scale. Steeper topographic convergence in the upper watershed may lead to old, near-surface groundwater that is taken up by vegetation for transpiration or lost through evaporation. Lower in the watershed, the relatively flat topography and deeper groundwater tables mean older groundwater is not available for ET; instead, precipitation and irrigation (see Section 3.1) are evapotranspired before they infiltrate down to deeper groundwater.

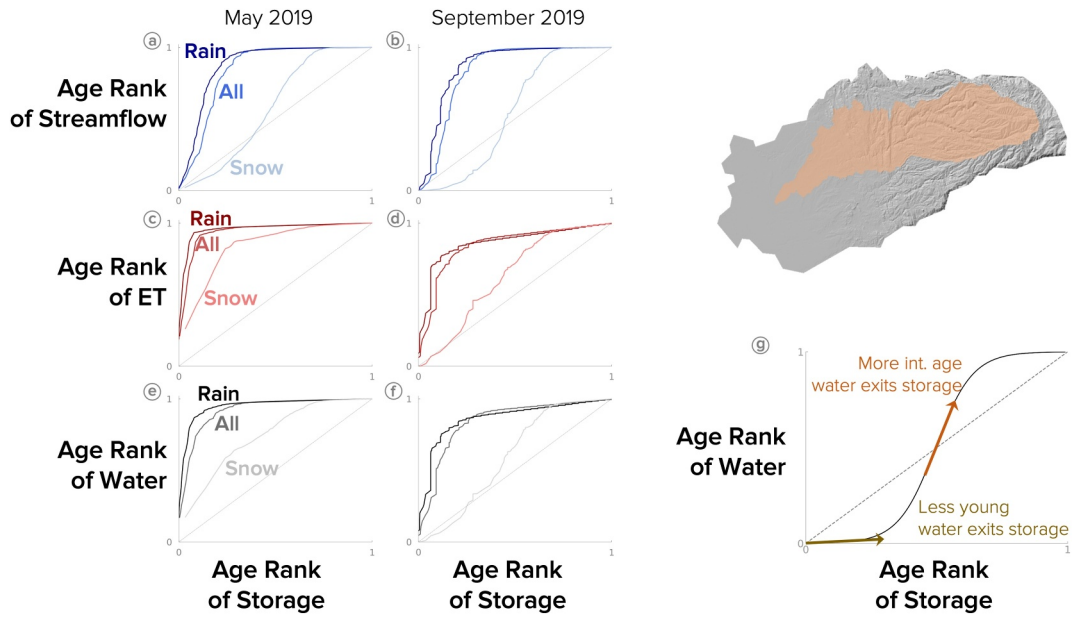

Figure 7. Storage selection curves of simulated streamflow (a, b) in blue, evapotranspiration (c, d) in red, and the total water lost (streamflow and evapotranspiration; e, f) in gray for May 2019 (a, c, e) and September 2019 (b, d, f) for the watershed defined by the river at Mahon Ranch, shown in tan on the shaded relief map at the right. Darker colors indicate water that originated as rain, the lightest color indicates water that originated as snow, and the middle color indicates the sum of the two. The 1:1 line is shown as a light gray dashed line. As shown in (g), storage selection curves represent the relative age of water in storage versus that lost to streamflow or evapotranspiration. Line sections that are steeper than the 1:1 line represent more water exiting storage in that age band than is being kept in storage; lines that are less steep than the 1:1 line represent less water exiting storage in that age band than is being kept in storage. Here we see that streamflow preferentially takes slightly older water from the "young water" component, but younger water from the "old water" component, both in May and September, though more significantly in May, while streamflow that originates as rain is generally much younger than the water in storage, weighting all streamflow to be younger than storage. Evapotranspiration is generally much younger than storage, particularly in May. The evapotranspiration from snow line goes above the rain line at older storage ages, suggesting that old water that began as snow is less likely to exit than old water that began as rain. The total water lost looks more like rain because much of the watershed's precipitation falls as rain.

Baseflow and snowmelt dynamics demonstrate key seasonal changes in the age distributions of both streamflow and ET in the model, particularly in the Camp Creek, North Fork, and Middle Fork headwaters. Early in the water year, nearly all streamflow is from previous water years. During snowmelt (a period of about 6 weeks), streamflow increases steeply mostly with water from the current water year, though there is also a small increase in older water. After snowmelt, streamflow is again dominated by water that fell before the current water year as seen by the current year's flat cumulative streamflow curves. In contrast, early year ET is split nearly evenly between current water year and older water. During snowmelt, ET increases primarily with current-water-year water, including a sizable fraction of water that infiltrated during the last five days. After snowmelt, ET comes primarily from water that fell within the water year.

The seasonal changes in water ages for simulated streamflow and ET are further illustrated by the cumulative age distributions of water that exits the watershed (Figure 6). In May 2019, streamflow is substantially older than ET; ET consists almost solely of water from the current water year while streamflow has substantial sources from the last 5 years. Streamflow has a similar, though slightly older, distribution in September compared to May. In contrast, the ET age distribution shifts substantially from May to September, with the September ET including much more water from previous water years. September ET also sees a substantial divergence in the age distribution of water that fell as rain versus snow, with most very young ET and a long tail of older ET both having fallen as rain. Streamflow sees only a small difference in water's age distribution across precipitation phases between May and September.

3.3. Selection of Water Storage

Simulated streamflow and ET are generally younger than the modeled water in storage in the Cosumnes, both during peak flow (May 2019) and the dry season (September 2019), though somewhat older water is selected from storage both in September and for snow-derived streamflow (Figure 7). Figure 7's fractional age-ranked storage selection (fSAS) functions plot the CDF of the age of water exiting the system (as streamflow, ET, or total) vertically against the CDF of the age of water in storage horizontally, as discussed in Section 2.4.3. These curves provide information about the age of streamflow and ET relative to the storage water, rather than the absolute age discussed in Section 3.2. The ET and streamflow volumes are also split by precipitation source phase (rain/snow) and compared to water in storage with the same source phase. Note that less water leaves the system in September than in May, and thus is represented by many fewer particles and the curves are much less smooth.

Simulated streamflow is younger than water in storage in both May and September. As discussed before, in both months only a very small fraction of streamflow is older than 5 years (Figure 6), while about 65% of storage is older than 5 years. The SAS curves for rain-derived streamflow are very similar to the overall SAS curve. In contrast, the snow-derived streamflow SAS function is well below the 1:1 uniform selection diagonal, showing that snow-derived streamflow contains a smaller proportion of the youngest water in snow storage (less than 6 months in May or 1 year in September). This difference between streamflow SAS functions implies that the age distribution of snow-derived storage is different from that of rain-derived storage since the age distributions of rain- and snow-derived streamflow are nearly identical (Figure 6). In particular, snow-derived storage appears to be younger than rain-derived storage and appears to occupy a smaller volume than rain-derived storage. Simulated streamflow is selecting older water from snow-derived storage, perhaps through a piston flow mechanism at higher watershed elevations. In contrast, rain-derived streamflow is young relative to rain-derived storage across all age ranges and does not show the same preference for slightly older water. The phase-differentiated SAS curves clearly illustrate the distinct differences in behavior between steep, high-elevation, snow-dominated headwaters and lower slope, low-elevation, rain-dominated parts of the watershed.

ET is younger than water in storage in both May and September in the model, and ET selects even younger water from storage than streamflow. The preference of ET to remove the youngest water in storage is stronger for rain-derived storage than for snow-derived storage. In May, ET removes only the youngest water from storage as seen by the near-vertical line to >0.9 of the age rank of ET. Snow-derived May ET is also younger than the snow-derived storage, as seen by the line that is steeper than the 1:1 up to 6 months in age or ∼0.2 of age rank of storage. The slope breakpoint in the snow-derived ET SAS function at about 6 months suggests ET may effectively draw from two pools of snow-derived storage: snow-derived storage younger than 6 months is preferentially selected as ET but snow-derived storage older than 6 months is removed more evenly up to the oldest water in storage. In September, most ET is derived from rain and again largely selects the youngest water in storage. In this month, about 15% of ET is contributed by a broad spectrum of older storage water. The SAS function of snow-derived September ET shows three segments. Snow-derived ET appears to be uniformly selected from the snow-derived storage for the younger than 6 months old as seen by it falling on the 1:1 line. ET then preferentially selects water older than 6 months but younger than ∼5 years from snow storage. Finally, there is a small contribution of the oldest snow in storage to September ET. Comparing the shape of the SAS ET functions, the May curve appears similar to the September curve, but with a very large additional component of the youngest water in storage.

4. Discussion

4.1. Understanding Watershed Behavior From *Age* and *Phase* Perspectives

"*Accurate prediction of the headwater hydrograph implies adequate modeling of sources, flowpaths and residence time of water and solutes*." (Hewlett & Troendle, 1975).

Observations that mean travel times in watersheds often exceed the hydrological response time by orders of magnitude (Martinec, 1975) has spurred many studies into the double paradox of rapid mobilization but apparently old water in streams, based on variable chemistry (Kirchner, 2003). Hillslope-scale flow and transport simulations (Jones et al., 2006) have demonstrated the role of hydrodynamic mixing in mobilizing pre-event water while storage selection approaches (Rinaldo et al., 2015) have provided deeper insights into watershed-scale processes

generating streamflow. SAS models have been supported by numerous isotopic and chemical tracer studies at the experimental (Kim et al., 2016; Pangle et al., 2017), hillslope (Kim & Harman, 2022), and watershed scale (Rinaldo et al., 2015; Van der Velde et al., 2012; van der Velde et al., 2015; Visser et al., 2019). Recently, observations of isotopically distinct sources of water in soil, streamflow, and xylem have driven study into how precipitation source phase affects watershed function (e.g., Brooks et al., 2010; Sprenger et al., 2016, 2022). Until now, computational infrastructure limited the numerical examination of storage selection and precipitation source phase behavior to experimental (Pangle et al., 2017), hillslope (Kim & Harman, 2022), and research catchment scales (Wilusz et al., 2020) with a few exceptions that have other limitations (Glaser et al., 2021; Jing et al., 2021; Weill et al., 2019).

Our work is the first to demonstrate how watershed-scale particle-tracking simulation enables analysis of water ages, storage selection behavior, and source partitioning in unparalleled detail. This approach can examine long-term average behavior of the whole watershed, or focus on specific locations (e.g., sample locations) or key moments (e.g., peak snow melt or late summer base flow). In our simulations, both streamflow and evapotranspiration prefer to select the youngest water from storage, consistent with previous work suggesting that much streamflow around the globe consists of young water (Jasechko et al., 2016). This effect is stronger than observed in periodic-steady-state simulations of a 1 m^3 lysimeter with periodic tracer applications (Kim et al., 2016; Pangle et al., 2017) where young water supplied larger fractions of streamflow when the water table rose near the surface. The snow-derived storage selection curves in our model show a preference for somewhat older water from storage, consistent with a tracer-based analysis of a Southern Sierra Nevada headwater catchment (Visser et al., 2019). That catchment exhibited a preference for older water discharge during low-flow conditions and only a slight preference for younger water during high flow conditions. We attribute the strong preference to discharge the youngest rain-derived water from storage in our model to (a) the larger volume of rain-derived water in storage at lower watershed elevations, and (b) the absence of local dispersion and diffusion in our simulations (Jones et al., 2006) which could decrease the contribution of event water. We hypothesize that explicitly accounting for dispersion along simulated flow paths to reflect real-world dispersion will reduce the preference for the youngest water in storage. This effect is expected to be stronger in regions with high contrasts in permeability and high anisotropy (Siirila & Maxwell, 2012). Importantly, we expect that accurately reproducing watershed-scale storage selection behavior will build a deeper understanding of subsurface structure, since the latter controls steady-state hillslope behavior (Kim et al., 2022).

Snow preferentially exits as streamflow and rain preferentially exits as evapotranspiration (ET) in our simulations. We propose three reasons this split might occur: (a) lower energy availability in snow-dominated conditions results in a larger streamflow generation while higher energy availability in rain conditions produces more soil evaporation and transpiration; (b) persistent snowmelt into high-antecedent moisture soils enhances flow and connections to streams and groundwater; and (c) snow preferentially falls in headwaters with a lower-hydraulic conductivity subsurface, driving more runoff. Our work is consistent with an emerging view that snow disproportionally contributes to streamflow, while water from rain remains relatively stationary and contributes primarily to ET (Carroll et al., 2020; Hammond et al., 2019; Li et al., 2017; Siirila-Woodburn et al., 2023; Sprenger et al., 2022). Ongoing work is comparing dynamic-flux particle tracking results to these isotope measurements in a mountain watershed where the precipitation source phase partitioning appears linked to tree density and aspect (Sprenger et al., 2022). In a warmer low-to-no-snow future, vegetation may have access to a larger fraction of the water budget, leaving a smaller fraction for streamflow (Maina et al., 2022).

4.2. Management Application

To manage water resources in a changing climate, we need to understand the ecohydrologic processes that provide water for both people and nature. Dynamic-flux particle tracking enables a better understanding of hydrologic fluxes at the watershed scale via novel in-depth analyses of the modeled streamflow and ET pathways, differentiated by source phase and age with spatially-variable groundwater contributions. Our simulations demonstrate two features of watershed behavior with potentially critical implications for water resource management.

First, we find that snow preferentially exits as streamflow and rain preferentially exits as ET in the simulation. If streamflow is substantially reduced in a low-to-no-snow future (Siirila-Woodburn et al., 2021), it may limit the

ability of current plans to store larger amounts of streamflow in dams and the subsurface to provide resilience against the loss of snowpack (Dahlke et al., 2018; Perrone & Rohde, 2016). At the same time, we expect that rain and snow partitioning may shift as more intense precipitation events increase the portion of rain rapidly entering streamflow. Dynamic-flux particle tracking simulations of future climate scenarios can assess the magnitude of these changes to determine appropriate management adaptations.

Second, the oldest water in storage seems to be removed primarily by ET in September. This may indicate that ET accesses *long* flow paths in convergent zones, which could make vegetation along streams and in meadows resilient to drought as the flow paths integrate a large distribution of water ages. Alternately, that old water might indicate *slow* flow paths due to low permeability/porosity of the subsurface, which would be less resilient because the shorter slow flow paths will store and provide less water. Understanding such details will be a critical part of managing water in a future where increasing temperature will alter both water source phase and the energy available for ET.

Dynamic-flux particle tracking also provides new opportunities to communicate scientific results to stakeholders and watershed communities. The movement of distinct packets of water is a more intuitive representation than classic watershed budget metrics, and the water source wedges we present here provide one intuitive way to demonstrate the flow of this water with high information density. When properly integrated in a decision-making framework with stakeholders, dynamic-flux particle tracking may help efficiently inform management options related to reservoir operations, headwaters-to-groundwater water storage planning including managed-aquifer recharge, achieving environmental resilience, and landscape management.

4.3. Future Research

Here, we demonstrate how dynamic-flux particle tracking simulations can interrogate watershed function at a level of detail that is not feasible by field measurements and observations. Dynamic-flux particle tracking can also constrain simulations by providing information on the distinct simulated flow paths of water that are more sensitive to detailed watershed processes and conditions than integrated measures such as streamflow. Because dynamic-flux particles represent specific packets of water that flow through the subsurface, dynamic-flux particle tracking results are ideally suited to compare to hydrologic tracer measurements that reflect the integrated effects of watershed-scale flow processes and transit time. For example, analyses could compare dynamic-flux model outputs with stable isotope measurements of streamflow and groundwater to test whether the simulation correctly links the precipitation source phase or input elevations with water's exit phase. Simulated subsurface residence time and its intra-annual variation could be compared to measurements of naturally occurring radioactive isotopes that are sensitive to different periods of water's residence time to understand how watersheds select water from storage for streamflow. Comparing dynamic flux particle tracking with measured isotopic or other chemical or biological tracer concentrations could also aid in identifying whether the numerical models are sufficiently accurate representations of the real watershed. In addition, we could better understand the uncertainty in our simulations and interpretations of watershed function by investigating the range of ages and water sources estimated from dynamic-flux particle tracking using different model parameterizations of both subsurface structure and land surface processes.

4.4. Model Limitations

While this work demonstrates valuable new approaches to investigate watershed function, this application has important limitations that should be considered when interpreting the results. First, previous work developed the watershed simulation of the Cosumnes Watershed that we used to drive the dynamic-flux particle tracking. The comparison of the simulation outputs to observations and satellite data products suggests that the simulation reasonably represents watershed processes. However, complex watershed simulators like ParFlow-CLM remain too computationally costly to formally calibrate to observations. At the moment, we lack observational data that could constrain the particle tracking results. Therefore, we present the results here as model outputs illustrating watershed behavior rather than precise metrics about how the Cosumnes Watershed functions. We note that these simulation outputs are consistent with observations in other Western US mountain watersheds, but acknowledge the lack of formal constraints on this particular watershed.

We further acknowledge several limitations in the models themselves. EcoSLIM tracks water particles only through subsurface flow, and the version used here did not yet include the addition of particles through

lateral boundaries. Therefore, the model does not account for water that never enters the subsurface nor that enters or exits through the lateral boundary conditions. Because the transit time of water through the stream network is much faster than through the subsurface, it is unlikely to substantially change our results. The lateral boundaries are unlikely to substantially affect results because the simulated domain is substantially larger than the topographic watershed boundary. Further, the ages presented here reflect the time since infiltration. Therefore, the snow age is that since melt, rather than since snowfall. Including a model that accurately tracks the age of snowmelt could add important information regarding the distinct behavior of different snowfall regimes. In recent work we applied an age correction to snowfall that assumes a perfect mixing of snow through the melt process (Siirila-Woodburn et al., 2023), but more sophisticated mixing models might be appropriate given complex snow melt processes. Finally, while ParFlow-CLM has been used to understand key surface/subsurface interactions (Condon & Maxwell, 2019; Maxwell & Kollet, 2008; Schreiner-McGraw & Ajami, 2020), the representation of evapotranspiration, and the partitioning between evaporation and transpiration, remain limited. Recent work to couple ParFlow with more advanced vegetation representations (Fang et al., 2022) can improve on these representations, and future work could investigate the role of these representations in affecting water's simulated flow paths. We discuss these potential shortcomings in more detail in Supplement S.2.

5. Conclusions

We demonstrate the novel capabilities of dynamic-flux particle tracking to elucidate details of watershed function that are difficult to interrogate with traditional methods in integrated watershed models, and illustrate these capabilities with a novel visualization we call water source wedges. We further discuss how insight gained from this new approach can help understand watershed dynamics. We detail these methods by applying them to a representative California watershed (Maina et al., 2020). To our knowledge this is the first application of this approach at large watershed scale, likely because the 700M particle simulation over more than 1M simulation cells requires substantial computational effort. The final watershed and dynamic-flux particle simulation which was analyzed here required more than 18,000 core hr and about 1.5 TB of storage, after an extensive spinup simulation that required 2x more resources. This work demonstrates how dynamic-flux particle tracking can help us understand how integrated watershed simulators function and, with proper constraints, how watersheds function. Such techniques will help drive future knowledge about watershed behavior and how it will shift in a changing climate.

In our simulations, streamflow is primarily derived from water that fell as snow while evapotranspiration (ET) is generally derived from water that fell as rain (Figure 3). This difference in precipitation source phase reflects a strong elevational gradient in the watershed, in which the upper watershed receives much more precipitation as snow while the lower watershed receives less water with precipitation in the form of rain. In addition, the lower watershed has substantially higher temperatures, and hence more energy demand for ET. This can be seen in the distinct source elevations of streamflow, which mostly starts above 1,000 m, and ET, which is sourced relatively evenly across the watershed (Figure 4).

The simulation also shows distinct differences in the age distributions of streamflow and ET; ET is generally younger than streamflow but also accounts for most of the oldest water leaving the watershed (Figure 5). Streamflow consists primarily of water that fell before the current water year though within the last 5 years, while ET water primarily fell within the current water year. The age of exiting water also shows the effect of the elevation gradient. Streamflow age distributions do not show elevational trends and are consistent across the watershed, in part because little of the precipitation that falls in the lower watershed leaves as streamflow. In contrast, ET has a much larger fraction of old water in the headwaters than at lower elevations, likely because either (a) the steep topography leads to flow paths that converge along streams where vegetation can access the water, and/or because (b) low-permeability and porosity bedrock in the headwaters slows the high-elevation groundwater which is thus older.

Finally, our simulation also shows that the water exiting as both ET and streamflow is generally younger than water in storage (Figure 7). ET is particularly young relative to storage, though it also includes a small component of relatively old water, likely in the topographic convergent zones discussed above. In contrast, streamflow derived from snow preferentially selects water between 1 and 5 years old during the dry season, suggesting intermediate system memory and multi-year buffering capacity. Further work should consider the

time periods of these system dynamics, especially as multi-year droughts and transitions in climate force more persistent perturbations.

Conflict of Interest

The authors declare no conflicts of interest relevant to this study.

Data Availability Statement

Model simulations were performed with open-source software: ParFlow-CLM version 3.9.0 available at https://github.com/parflow and an adapted EcoSLIM version 1.3 available at https://github.com/pjdf/EcoSLIM. Scripts used to run simulations and create figure panels are being made available through a Zenodo repository at https://doi.org/10.5281/zenodo.10667904 (Dennedy-Frank, 2024). Simulation outputs involve more than 1 TB of data. It is currently impracticable to archive such large data sets in a repository, so we have supplied all the information needed to replicate the simulations and analysis through these scripts.

Acknowledgments
We thank two anonymous reviewers for their thoughtful comments on this work. This research used resources of the National Energy Research Scientific Computing Center (NERSC), a US Department of Energy Office of Science User Facility located at Lawrence Berkeley national Laboratory, operated under contract no. DE-AC02-05CH11231. Researchers Dennedy-Frank and Siirila-Woodburn at Lawrence Berkeley National Laboratory were supported by the US Department of Energy Grant DE-AC02-05CH11231. Work by researcher Visser at Lawrence Livermore National Laboratory was performed under the auspices of the U. S. Department of Energy under Contract DE-AC52-07NA27344 with funding from the University of California Collaborative Research and Training Award LFR-18-548316 and LLNL-JRNL-851127.

References

Allen, R. G., Tasumi, M., & Trezza, R. (2007). Satellite-based energy balance for mapping evapotranspiration with internalized calibration (METRIC)—Model. *Journal of Irrigation and Drainage Engineering*, *133*(4), 380–394. https://doi.org/10.1061/(ASCE)0733-9437(2007)133:4(380)

Barnett, T. P., Adam, J. C., & Lettenmaier, D. P. (2005). Potential impacts of a warming climate on water availability in snow-dominated regions. *Nature*, *438*(7066), 303–309. https://doi.org/10.1038/nature04141

Benettin, P., Rodriguez, N. B., Sprenger, M., Kim, M., Klaus, J., Harman, C. J., et al. (2022). Transit time estimation in catchments: Recent developments and future directions. *Water Resources Research*, *58*(11), e2022WR033096. https://doi.org/10.1029/2022WR033096

Berghuijs, W. R., Woods, R. A., & Hrachowitz, M. (2014). A precipitation shift from snow towards rain leads to a decrease in streamflow. *Nature Climate Change*, *4*(7), 583–586. https://doi.org/10.1038/nclimate2246

Beven, K., & Freer, J. (2001). Equifinality, data assimilation, and uncertainty estimation in mechanistic modelling of complex environmental systems using the GLUE methodology. *Journal of Hydrology*, *249*(1–4), 11–29. https://doi.org/10.1016/S0022-1694(01)00421-8

Brooks, J. R., Barnard, H. R., Coulombe, R., & McDonnell, J. J. (2010). Ecohydrologic separation of water between trees and streams in a Mediterranean climate. *Nature Geoscience*, *3*(2), 100–104. https://doi.org/10.1038/ngeo722

Brunner, P., & Simmons, C. T. (2012). HydroGeoSphere: A fully integrated, physically based hydrological model. *Ground Water*, *50*(2), 170–176. https://doi.org/10.1111/j.1745-6584.2011.00882.x

Carroll, R. W. H., Gochis, D., & Williams, K. H. (2020). Efficiency of the summer monsoon in generating streamflow within a snow-dominated headwater basin of the Colorado River. *Geophysical Research Letters*, *47*(23), e2020GL090856. https://doi.org/10.1029/2020GL090856

Condon, L. E., & Maxwell, R. M. (2019). Simulating the sensitivity of evapotranspiration and streamflow to large-scale groundwater depletion. *Science Advances*, *5*(6), eaav4574. https://doi.org/10.1126/sciadv.aav4574

Crouzet, E., Hubert, P., Olive, P., Siwertz, E., & Marce, A. (1970). Le tritium dans les mesures d'hydrologie de surface. Determination experimentale du coefficient de ruissellement. *Journal of Hydrology*, *11*(3), 217–229. https://doi.org/10.1016/0022-1694(70)90063-6

Dahlke, H. E., LaHue, G. T., Mautner, M. R. L., Murphy, N. P., Patterson, N. K., Waterhouse, H., et al. (2018). Chapter eight - Managed aquifer recharge as a tool to enhance sustainable groundwater management in California: Examples from field and modeling studies. In J. Friesen & L. Rodríguez-Sinobas (Eds.), *Advances in chemical pollution, environmental management and protection* (Vol. 3, pp. 215–275). Elsevier. https://doi.org/10.1016/bs.apmp.2018.07.003

Dai, Y., Zeng, X., Dickinson, R. E., Baker, I., Bonan, G. B., Bosilovich, M. G., et al. (2003). The common land model. *Bulletin of the American Meteorological Society*, *84*(8), 1013–1024. https://doi.org/10.1175/BAMS-84-8-1013

Danesh-Yazdi, M., Klaus, J., Condon, L. E., & Maxwell, R. M. (2018). Bridging the gap between numerical solutions of travel time distributions and analytical storage selection functions. *Hydrological Processes*, *32*(8), 1063–1076. https://doi.org/10.1002/hyp.11481

Davenport, F. V., Herrera-Estrada, J. E., Burke, M., & Diffenbaugh, N. S. (2020). Flood size increases nonlinearly across the Western United States in response to lower snow-precipitation ratios. *Water Resources Research*, *56*(1), e2019WR025571. https://doi.org/10.1029/2019WR025571

Dennedy-Frank, P. J. (2024). Cosumnes EcoSLIM simulation for JAMES [Software]. *Zenodo*. https://doi.org/10.5281/zenodo.10667904

Dettinger, M. D., Ralph, F. M., Das, T., Neiman, P. J., & Cayan, D. R. (2011). Atmospheric rivers, floods and the water resources of California. *Water*, *3*(2), 445–478. https://doi.org/10.3390/w3020445

Dunne, T., & Black, R. D. (1970). Partial area contributions to storm runoff in a small New England watershed. *Water Resources Research*, *6*(5), 1296–1311. https://doi.org/10.1029/WR006i005p01296

Earman, S., Campbell, A. R., Phillips, F. M., & Newman, B. D. (2006). Isotopic exchange between snow and atmospheric water vapor: Estimation of the snowmelt component of groundwater recharge in the southwestern United States. *Journal of Geophysical Research*, *111*(D9), D09302. https://doi.org/10.1029/2005JD006470

Engdahl, N. B., & Maxwell, R. M. (2015). Quantifying changes in age distributions and the hydrologic balance of a high-mountain watershed from climate induced variations in recharge. *Journal of Hydrology*, *522*, 152–162. https://doi.org/10.1016/j.jhydrol.2014.12.032

Fang, Y., Leung, L. R., Koven, C. D., Bisht, G., Detto, M., Cheng, Y., et al. (2022). Modeling the topographic influence on aboveground biomass using a coupled model of hillslope hydrology and ecosystem dynamics. *Geoscientific Model Development*, *15*(20), 7879–7901. https://doi.org/10.5194/gmd-15-7879-2022

Freeze, R. A., & Harlan, R. L. (1969). Blueprint for a physically-based, digitally-simulated hydrologic response model. *Journal of Hydrology*, *9*(3), 237–258. https://doi.org/10.1016/0022-1694(69)90020-1

Geologic Map of California. (2015). Retrieved from https://maps.conservation.ca.gov/cgs/gmc/

Glaser, B., Hopp, L., Partington, D., Brunner, P., Therrien, R., & Klaus, J. (2021). Sources of surface water in space and time: Identification of delivery processes and geographical sources with hydraulic mixing-cell modeling. *Water Resources Research*, *57*(12), e2021WR030332. https://doi.org/10.1029/2021WR030332

Hammond, J. C., Harpold, A. A., Weiss, S., & Kampf, S. K. (2019). Partitioning snowmelt and rainfall in the critical zone: Effects of climate type and soil properties. *Hydrology and Earth System Sciences*, *23*(9), 3553–3570. https://doi.org/10.5194/hess-23-3553-2019

Harman, C. J. (2019). Age-ranked storage-discharge relations: A unified description of spatially lumped flow and water age in hydrologic systems. *Water Resources Research*, *55*(8), 7143–7165. https://doi.org/10.1029/2017WR022304

Heppner, C. S., & Loague, K. (2008). A dam problem: Simulated upstream impacts for a Searsville-like watershed. *Ecohydrology*, *1*(4), 408–424. https://doi.org/10.1002/eco.34

Hewlett, J. D., & Troendle, C. A. (1975). Non point and diffused water sources: A variable source area problem. In *Watershed management: Proceedings of a symposium* (pp. 21–46).

Homer, C., Dewitz, J., Yang, L., Jin, S., Danielson, P., Coulston, J., et al. (2015). Completion of the 2011 national land cover database for the conterminous United States – Representing a decade of land cover change information. *Photogrammetric Engineering*, *10*.

Jasechko, S., Kirchner, J. W., Welker, J. M., & McDonnell, J. J. (2016). Substantial proportion of global streamflow less than three months old. *Nature Geoscience*, *9*(2), 126–129. https://doi.org/10.1038/ngeo2636

Jennings, C. W., Strand, R. G., & Rogers, T. H. (1977). Geologic map of California.

Jing, M., Kumar, R., Attinger, S., Li, Q., Lu, C., & Heße, F. (2021). Assessing the contribution of groundwater to catchment travel time distributions through integrating conceptual flux tracking with explicit Lagrangian particle tracking. *Advances in Water Resources*, *149*, 103849. https://doi.org/10.1016/j.advwatres.2021.103849

Jones, J. P., Sudicky, E. A., Brookfield, A. E., & Park, Y.-J. (2006). An assessment of the tracer-based approach to quantifying groundwater contributions to streamflow. *Water Resources Research*, *42*(2), W02407. https://doi.org/10.1029/2005WR004130

Kim, M., & Harman, C. J. (2022). Transit times and StorAge selection functions in idealized hillslopes with steady infiltration. *Water Resources Research*, *58*(5), e2019WR025917. https://doi.org/10.1029/2019WR025917

Kim, M., Pangle, L. A., Cardoso, C., Lora, M., Volkmann, T. H. M., Wang, Y., et al. (2016). Transit time distributions and StorAge selection functions in a sloping soil lysimeter with time-varying flow paths: Direct observation of internal and external transport variability: Variable transit time experiment. *Water Resources Research*, *52*(9), 7105–7129. https://doi.org/10.1002/2016WR018620

Kim, M., Volkmann, T. H. M., Wang, Y., Meira Neto, A. A., Matos, K., Harman, C. J., & Troch, P. A. (2022). Direct observation of hillslope scale StorAge selection functions in experimental hydrologic systems: Geomorphologic structure and preferential discharge of old water. *Water Resources Research*, *58*(3), e2020WR028959. https://doi.org/10.1029/2020WR028959

Kirchner, J. W. (2003). A double paradox in catchment hydrology and geochemistry. *Hydrological Processes*, *17*(4), 871–874. https://doi.org/10.1002/hyp.5108

Kirchner, J. W., & Allen, S. T. (2020). Seasonal partitioning of precipitation between streamflow and evapotranspiration, inferred from end-member splitting analysis. *Hydrology and Earth System Sciences*, *24*(1), 17–39. https://doi.org/10.5194/hess-24-17-2020

Klaus, J., & McDonnell, J. J. (2013). Hydrograph separation using stable isotopes: Review and evaluation. *Journal of Hydrology*, *505*, 47–64. https://doi.org/10.1016/j.jhydrol.2013.09.006

Kollet, S. J., & Maxwell, R. M. (2006). Integrated surface–groundwater flow modeling: A free-surface overland flow boundary condition in a parallel groundwater flow model. *Advances in Water Resources*, *29*(7), 945–958. https://doi.org/10.1016/j.advwatres.2005.08.006

Kollet, S. J., & Maxwell, R. M. (2008). Demonstrating fractal scaling of baseflow residence time distributions using a fully-coupled groundwater and land surface model. *Geophysical Research Letters*, *35*(7), L07402. https://doi.org/10.1029/2008GL033215

Kollet, S. J., Maxwell, R. M., Woodward, C. S., Smith, S., Vanderborght, J., Vereecken, H., & Simmer, C. (2010). Proof of concept of regional scale hydrologic simulations at hydrologic resolution utilizing massively parallel computer resources. *Water Resources Research*, *46*(4), W04201. https://doi.org/10.1029/2009WR008730

Li, D., Wrzesien, M. L., Durand, M., Adam, J., & Lettenmaier, D. P. (2017). How much runoff originates as snow in the western United States, and how will that change in the future? Western U.S. Snowmelt-Derived Runoff. *Geophysical Research Letters*, *44*(12), 6163–6172. https://doi.org/10.1002/2017GL073551

Loague, K., Heppner, C. S., Abrams, R. H., Carr, A. E., VanderKwaak, J. E., & Ebel, B. A. (2005). Further testing of the Integrated Hydrology Model (InHM): Event-based simulations for a small rangeland catchment located near Chickasha, Oklahoma. *Hydrological Processes*, *19*(7), 1373–1398. https://doi.org/10.1002/hyp.5566

Maina, F. Z., Rhoades, A., Siirila-Woodburn, E. R., & Dennedy-Frank, P.-J. (2022). Projecting end-of-century climate extremes and their impacts on the hydrology of a representative California watershed. *Hydrology and Earth System Sciences*, *26*(13), 3589–3609. https://doi.org/10.5194/hess-26-3589-2022

Maina, F. Z., & Siirila-Woodburn, E. R. (2019). Watersheds dynamics following wildfires: Nonlinear feedbacks and implications on hydrologic responses. *Hydrological Processes*, *34*(1), 33–50. https://doi.org/10.1002/hyp.13568

Maina, F. Z., Siirila-Woodburn, E. R., Newcomer, M., Xu, Z., & Steefel, C. (2020). Determining the impact of a severe dry to wet transition on watershed hydrodynamics in California, USA with an integrated hydrologic model. *Journal of Hydrology*, *580*, 124358. https://doi.org/10.1016/j.jhydrol.2019.124358

Martinec, J. (1975). Subsurface flow from snowmelt traced by tritium. *Water Resources Research*, *11*(3), 496–498. https://doi.org/10.1029/WR011i003p00496

Maxwell, R. M. (2013). A terrain-following grid transform and preconditioner for parallel, large-scale, integrated hydrologic modeling. *Advances in Water Resources*, *53*, 109–117. https://doi.org/10.1016/j.advwatres.2012.10.001

Maxwell, R. M., & Condon, L. E. (2016). Connections between groundwater flow and transpiration partitioning. *Science*, *353*(6297), 377–380. https://doi.org/10.1126/science.aaf7891

Maxwell, R. M., Condon, L. E., Danesh-Yazdi, M., & Bearup, L. A. (2019). Exploring source water mixing and transient residence time distributions of outflow and evapotranspiration with an integrated hydrologic model and Lagrangian particle tracking approach. *Ecohydrology*, *12*(1), e2042. https://doi.org/10.1002/eco.2042

Maxwell, R. M., & Kastenberg, W. E. (1999). Stochastic environmental risk analysis: An integrated methodology for predicting cancer risk from contaminated groundwater. *Stochastic Environmental Research and Risk Assessment*, *13*(1–2), 27–47. https://doi.org/10.1007/s004770050030

Maxwell, R. M., & Kollet, S. J. (2008). Interdependence of groundwater dynamics and land-energy feedbacks under climate change. *Nature Geoscience*, *1*(10), 665–669. https://doi.org/10.1038/ngeo315

Maxwell, R. M., & Miller, N. L. (2005). Development of a coupled land surface and groundwater model. *Journal of Hydrometeorology*, *6*(3), 233–247. https://doi.org/10.1175/JHM422.1

Maxwell, R. M., Welty, C., & Harvey, R. W. (2007). Revisiting the cape cod bacteria injection experiment using a stochastic modeling approach. *Environmental Science & Technology*, *41*(15), 5548–5558. https://doi.org/10.1021/es062693a

Meixner, T., Manning, A. H., Stonestrom, D. A., Allen, D. M., Ajami, H., Blasch, K. W., et al. (2016). Implications of projected climate change for groundwater recharge in the western United States. *Journal of Hydrology*, *534*, 124–138. https://doi.org/10.1016/j.jhydrol.2015.12.027

Milly, P. C. D., Betancourt, J., Falkenmark, M., Hirsch, R. M., Kundzewicz, Z. W., Lettenmaier, D. P., & Stouffer, R. J. (2008). Stationarity is dead: Whither water management? *Science*, *319*(5863), 573–574. https://doi.org/10.1126/science.1151915

Milly, P. C. D., & Dunne, K. A. (2020). Colorado River flow dwindles as warming-driven loss of reflective snow energizes evaporation. *Science*, *367*(6483), 1252–1255. https://doi.org/10.1126/science.aay9187

National Operational Hydrologic Remote Sensing Center. (2004). Snow data assimilation system (SNODAS) data products at NSIDC, version 1 [Dataset]. *National Snow and Ice Data Center*. https://doi.org/10.7265/N5TB14TC

Pangle, L. A., Kim, M., Cardoso, C., Lora, M., Meira Neto, A. A., Volkmann, T. H. M., et al. (2017). The mechanistic basis for storage-dependent age distributions of water discharged from an experimental hillslope: Mechanistic basis for age distributions. *Water Resources Research*, *53*(4), 2733–2754. https://doi.org/10.1002/2016WR019901

Perrone, D., & Rohde, M. M. (2016). Benefits and economic costs of managed aquifer recharge in California. *San Francisco Estuary and Watershed Science*, *14*(2). https://doi.org/10.15447/sfews.2016v14iss2art4

Pollock, D. W. (2012). *User guide for MODPATH version 6—A particle-tracking model for MODFLOW (U.S. Geological survey techniques and methods No. 6-A41)* (p. 58). U. S. Geological Survey. Retrieved from https://pubs.usgs.gov/tm/6a41/pdf/TM_6A_41.pdf

Reichle, R. H., Lannoy, G. J. M. D., Liu, Q., Koster, R. D., Kimball, J. S., Crow, W. T., et al. (2017). Global assessment of the SMAP level-4 surface and root-zone soil moisture product using assimilation diagnostics. *Journal of Hydrometeorology*, *18*(12), 3217–3237. https://doi.org/10.1175/JHM-D-17-0130.1

Rinaldo, A., Benettin, P., Harman, C. J., Hrachowitz, M., McGuire, K. J., van der Velde, Y., et al. (2015). Storage selection functions: A coherent framework for quantifying how catchments store and release water and solutes. *Water Resources Research*, *51*(6), 4840–4847. https://doi.org/10.1002/2015WR017273

Schreiner-McGraw, A. P., & Ajami, H. (2020). Impact of uncertainty in precipitation forcing data sets on the hydrologic budget of an integrated hydrologic model in mountainous terrain. *Water Resources Research*, *56*(12), e2020WR027639. https://doi.org/10.1029/2020WR027639

Schreiner-McGraw, A. P., & Ajami, H. (2022). Combined impacts of uncertainty in precipitation and air temperature on simulated mountain system recharge from an integrated hydrologic model. *Hydrology and Earth System Sciences*, *26*(4), 1145–1164. https://doi.org/10.5194/hess-26-1145-2022

Siirila, E. R., & Maxwell, R. M. (2012). Evaluating effective reaction rates of kinetically driven solutes in large-scale, statistically anisotropic media: Human health risk implications. *Water Resources Research*, *48*(4), W04527. https://doi.org/10.1029/2011WR011516

Siirila-Woodburn, E. R., Dennedy-Frank, P. J., Rhoades, A., Vahmani, P., Maina, F., Hatchett, B., et al. (2023). The role of atmospheric rivers on groundwater: Lessons learned from an extreme wet year. *Water Resources Research*, *59*(6), e2022WR033061. https://doi.org/10.1029/2022WR033061

Siirila-Woodburn, E. R., Fernàndez-Garcia, D., & Sanchez-Vila, X. (2015). Improving the accuracy of risk prediction from particle-based breakthrough curves reconstructed with kernel density estimators. *Water Resources Research*, *51*(6), 4574–4591. https://doi.org/10.1002/2014WR016394

Siirila-Woodburn, E. R., Rhoades, A. M., Hatchett, B. J., Huning, L. S., Szinai, J., Tague, C., et al. (2021). A low-to-no snow future and its impacts on water resources in the western United States. *Nature Reviews Earth & Environment*, *2*(11), 800–819. https://doi.org/10.1038/s43017-021-00219-y

Siirila-Woodburn, E. R., Sanchez-Vila, X., & Fernàndez-Garcia, D. (2015). On the formation of multiple local peaks in breakthrough curves. *Water Resources Research*, *51*(4), 2128–2152. https://doi.org/10.1002/2014WR015840

Siirila-Woodburn, E. R., Steefel, C. I., Williams, K. H., & Birkholzer, J. T. (2018). Predicting the impact of land management decisions on overland flow generation: Implications for cesium migration in forested Fukushima watersheds. *Advances in Water Resources*, *113*, 42–54. https://doi.org/10.1016/j.advwatres.2018.01.008

Sklash, M. G., Farvolden, R. N., & Fritz, P. (1976). A conceptual model of watershed response to rainfall, developed through the use of oxygen-18 as a natural tracer. *Canadian Journal of Earth Sciences*, *13*(2), 271–283. https://doi.org/10.1139/e76-029

Sprenger, M., Carroll, R. W. H., Dennedy-Frank, J., Siirila-Woodburn, E. R., Newcomer, M. E., Brown, W., et al. (2022). Variability of snow and rainfall partitioning into evapotranspiration and summer runoff across nine mountainous catchments. *Geophysical Research Letters*, *49*(13), e2022GL099324. https://doi.org/10.1029/2022GL099324

Sprenger, M., Leistert, H., Gimbel, K., & Weiler, M. (2016). Illuminating hydrological processes at the soil-vegetation-atmosphere interface with water stable isotopes. *Reviews of Geophysics*, *54*(3), 2015RG000515. https://doi.org/10.1002/2015RG000515

Sudicky, E. A., Jones, J. P., Park, Y.-J., Brookfield, A. E., & Colautti, D. (2008). Simulating complex flow and transport dynamics in an integrated surface-subsurface modeling framework. *Geosciences Journal*, *12*(2), 107–122. https://doi.org/10.1007/s12303-008-0013-x

Sulis, M., Paniconi, C., Rivard, C., Harvey, R., & Chaumont, D. (2011). Assessment of climate change impacts at the catchment scale with a detailed hydrological model of surface-subsurface interactions and comparison with a land surface model. *Water Resources Research*, *47*(1), W01513. https://doi.org/10.1029/2010WR009167

van der Velde, Y., Heidbüchel, I., Lyon, S. W., Nyberg, L., Rodhe, A., Bishop, K., & Troch, P. A. (2015). Consequences of mixing assumptions for time-variable travel time distributions. *Hydrological Processes*, *29*(16), 3460–3474. https://doi.org/10.1002/hyp.10372

Van der Velde, Y., Torfs, P. J. J. F., van der Zee, S. E. A. T. M., & Uijlenhoet, R. (2012). Quantifying catchment-scale mixing and its effect on time-varying travel time distributions. *Water Resources Research*, *48*(6), W06536. https://doi.org/10.1029/2011WR011310

Visser, A., Heerdink, R., Broers, H. P., & Bierkens, M. F. P. (2009). Travel time distributions derived from particle tracking in models containing weak sinks. *Groundwater*, *47*(2), 237–245. https://doi.org/10.1111/j.1745-6584.2008.00542.x

Visser, A., Kroes, J., van Vliet, M. T. H., Blenkinsop, S., Fowler, H. J., & Broers, H. P. (2012). Climate change impacts on the leaching of a heavy metal contamination in a small lowland catchment. *Journal of Contaminant Hydrology*, *127*(1–4), 47–64. https://doi.org/10.1016/j.jconhyd.2011.04.007

Visser, A., Thaw, M., Deinhart, A., Bibby, R., Safeeq, M., Conklin, M., et al. (2019). Cosmogenic isotopes unravel the hydrocarbonology and water storage dynamics of the Southern Sierra critical zone. *Water Resources Research*, *55*(2), 1429–1450. https://doi.org/10.1029/2018WR023665

Weill, S., Lesparre, N., Jeannot, B., & Delay, F. (2019). Variability of water transit time distributions at the strengbach catchment (Vosges Mountains, France) inferred through integrated hydrological modeling and particle tracking algorithms. *Water*, *11*(12), 2637. https://doi.org/10.3390/w11122637

Wilusz, D. C., Harman, C. J., Ball, W. P., Maxwell, R. M., & Buda, A. R. (2020). Using particle tracking to understand flow paths, age distributions, and the paradoxical origins of the inverse storage effect in an experimental catchment. *Water Resources Research*, *56*(4), e2019WR025140. https://doi.org/10.1029/2019WR025140

Yang, C., Maxwell, R. M., & Valent, R. (2022). Accelerating the Lagrangian simulation of water ages on distributed, multi-GPU platforms: The importance of dynamic load balancing. *Computers & Geosciences*, *166*, 105189. https://doi.org/10.1016/j.cageo.2022.105189

Yang, C., Ponder, C., Wang, B., Tran, H., Zhang, J., Swilley, J., et al. (2023). Accelerating the Lagrangian particle tracking in hydrologic modeling to continental-scale. *Journal of Advances in Modeling Earth Systems*, *15*(5), e2022MS003507. https://doi.org/10.1029/2022MS003507

Yang, C., Zhang, Y.-K., Liang, X., Olschanowsky, C., Yang, X., & Maxwell, R. (2021). Accelerating the Lagrangian particle tracking of residence time distributions and source water mixing towards large scales. *Computers & Geosciences*, *151*, 104760. https://doi.org/10.1016/j.cageo.2021.104760

Zhang, Y., Green, C. T., & Fogg, G. E. (2013). The impact of medium architecture of alluvial settings on non-Fickian transport. *Advances in Water Resources*, *54*, 78–99. https://doi.org/10.1016/j.advwatres.2013.01.004